

Time-causal and time-recursive spatio-temporal receptive fields*

Tony Lindeberg

Department of Computational Biology
School of Computer Science and Communication
KTH Royal Institute of Technology
SE-100 44 Stockholm, Sweden

Abstract

We present an improved model and theory for time-causal and time-recursive spatio-temporal receptive fields, obtained by a combination of Gaussian receptive fields over the spatial domain and first-order integrators or equivalently truncated exponential filters coupled in cascade over the temporal domain.

Compared to previous spatio-temporal scale-space formulations in terms of non-enhancement of local extrema or scale invariance, these receptive fields are based on different scale-space axiomatics over time by ensuring non-creation of new local extrema or zero-crossings with increasing temporal scale. Specifically, extensions are presented about (i) parameterizing the intermediate temporal scale levels, (ii) analysing the resulting temporal dynamics, (iii) transferring the theory to a discrete implementation in terms of recursive filters over time and (iv) computing scale-normalized spatio-temporal derivative expressions for spatio-temporal feature detection and (v) computational modelling of receptive fields in the lateral geniculate nucleus (LGN) and the primary visual cortex (V1) in biological vision.

We show that by distributing the intermediate temporal scale levels according to a logarithmic distribution, we obtain a new family of temporal scale-space kernels with better temporal characteristics compared to a more traditional approach of using a uniform distribution of the intermediate temporal scale levels. Specifically, the new family of time-causal kernels has much faster temporal response properties (shorter temporal delays) compared to the kernels obtained from a uniform distribution. With increasing number of temporal scale levels, the temporal scale-space kernels in the new family do also converge very rapidly to a limit kernel that possesses true self-similar scale invariant properties over temporal scales. Thereby, the new representation allows for true scale invariance over variations in the temporal scale, although the underlying temporal scale-space representation is based on a discretized temporal scale parameter.

We show how scale-normalized temporal derivatives can be defined for these time-causal scale-space kernels and how the composed theory can be used for computing basic types of scale-normalized spatio-temporal derivative expressions in a computationally efficient manner.

Keywords: scale space, receptive field, scale, spatial, temporal, spatio-temporal, scale-normalized derivative, scale invariance, feature detection, computer vision, computational modelling of biological vision

*The support from the Swedish Research Council (contract 2014-4083) is gratefully acknowledged.

Contents

1	Introduction	1
1.1	Organization of the presentation	2
2	Spatio-temporal receptive fields	3
3	Time-causal temporal scale-space	4
3.1	Time-causal scale-space kernels for pure temporal domain	4
3.2	Classification of scale-space kernels for continuous signals	5
3.3	Temporal scale-space kernels over continuous temporal domain	6
3.4	Temporal receptive fields	9
3.5	Computational modelling of biological receptive fields	11
3.6	Theoretical properties of time-causal spatio-temporal scale-space	12
4	Temporal dynamics of the time-causal kernels	13
5	The scale-invariant time-causal limit kernel	15
6	Computational implementation	18
6.1	Classification of scale-space kernels for discrete signals	18
6.2	Discrete temporal scale-space kernels based on recursive filters	19
6.3	Discrete implementation of spatial Gaussian smoothing	20
6.4	Discrete implementation of spatio-temporal receptive fields	21
7	Scale normalization for spatio-temporal derivatives	22
7.1	Scale normalization of spatial derivatives	22
7.2	Scale normalization of temporal derivatives	22
7.3	Computation of temporal scale normalization factors	24
7.4	Measuring the deviation from the scale-invariant limit kernel	25
8	Spatio-temporal feature detection	27
8.1	Partial derivatives	27
8.2	Directional derivatives	29
8.3	Differential invariants over spatial derivative operators	30
8.4	Space-time coupled spatio-temporal derivative expressions	31
8.5	Scale normalized spatio-temporal derivative expressions	35
8.6	Geometric covariance and invariance properties	36
8.7	Invariance to illumination variations and exposure control mechanisms	37
9	Summary and discussion	39
A	Frequency analysis of the time-causal kernels	41
A.1	Logarithmic distribution of the intermediate scale levels	42
A.2	Uniform distribution of the intermediate scale levels	43
B	Comparison with Koenderink's scale-time model	45

1 Introduction

Spatio-temporal receptive fields constitute an essential concept in biological vision (Hubel and Wiesel [28, 29, 30]; DeAngelis et al. [9, 8]) and for expressing computer vision methods on video data (Adelson and Bergen [1]; Zelnik-Manor and Irani [83]; Laptev and Lindeberg [39]; Jhuang et al. [32]; Shabani et al. [72]).

For off-line processing of pre-recorded video, non-causal Gaussian or Gabor-based spatio-temporal receptive fields may in some cases be sufficient. When operating on video data in a real-time setting or when modelling biological vision computationally, one does however need to take into explicit account the fact that the future cannot be accessed and that the underlying spatio-temporal receptive fields must be *time-causal*. For computational efficiency and for keeping down memory requirements, it is also desirable that the computations should be *time-recursive*, so that it is sufficient to keep a limited memory of the past that can be recursively updated over time.

The subject of this article is to present an improved scale-space model for spatio-temporal receptive fields based on time-causal temporal scale-space kernels in terms of first-order integrators or equivalently truncated exponential filters coupled in cascade, which can also be transferred to a discrete implementation in terms of recursive filters. The model builds on previous work by (Fleet and Langley [17]; Lindeberg and Fagerström [58]; Lindeberg [51, 52]) and will here be complemented by a better design for the degrees of freedom in the choice of time constants for the intermediate temporal scale levels, an analysis of the resulting temporal response dynamics and details for discrete implementation in a spatio-temporal visual front-end.

In previous use of the temporal scale-space model in (Lindeberg and Fagerström [58]), a uniform distribution of the intermediate scale levels was used when coupling first-order integrators or equivalently truncated exponential kernels in cascade. By instead using a logarithmic distribution of the intermediate scale levels, we will here show that a new family of temporal scale-space kernels can be obtained with much better properties in terms of (i) faster temporal response dynamics and (ii) fast convergence towards a limit kernel that possesses true scale-invariant properties (self-similarity) under variations in the temporal scale in the input data. Thereby, the new family of kernel enables (i) significantly shorter temporal delays (as always arise for truly time-causal operations), (ii) much better computational approximation to true temporal scale invariance and (iii) computationally much more efficient numerical implementation. Conceptually, our approach is also related to the time-causal scale-time model by Koenderink [36] which is here complemented by a truly time-recursive formulation of time-causal receptive fields more suitable for real-time operations over a compact temporal buffer of what has occurred in the past, including a theoretically well-founded and computationally efficient method for discrete implementation.

Specifically, the rapid convergence of the new family of temporal scale-space kernels to a limit kernel when the number of intermediate temporal scale levels tends to infinity is theoretically very attractive, since it provides a way to define truly scale-invariant operations over temporal variations at different temporal scales, and to measure the deviation from true scale invariance when approximating the limit kernel by a finite number of temporal scale levels. Thereby, the proposed model allows for truly self-similar temporal operations over temporal scales while using a discretized temporal scale parameter, which is a theoretically new type of construction for temporal scale spaces.

Based on a previously established analogy between scale-normalized derivatives for spatial derivative expressions and the interpretation of scale normalization of the

corresponding Gaussian derivative kernels to constant L_p -norms over scale (Lindeberg [49]), we will show how scale-invariant temporal derivative operators can be defined for the proposed new families of temporal scale-space kernels. Then, we will apply the resulting theory for computing basic spatio-temporal derivative expressions of different types and describe classes of such spatio-temporal derivative expressions that are invariant or covariant to basic types of natural image transformations, including independent rescaling of the spatial and temporal coordinates, illumination variations and variabilities in exposure control mechanisms.

In these ways, the proposed theory will present previously missing components for applying scale-space theory to spatio-temporal input data (video) based on truly time-causal and time-recursive image operations.

1.1 Organization of the presentation

To give the contextual overview to this work, section 2 starts by presenting a previously established computational model for spatio-temporal receptive fields in terms of spatial and temporal scale-space kernels, based on which we will replace the temporal smoothing step.

Section 3 starts by reviewing previously theoretical results for temporal scale-space models based on the assumption of non-creation of new local extrema with increasing scale, showing that the canonical temporal primitives in such a model are first-order integrators or equivalently truncated exponential kernels coupled in cascade. Relative to previous applications of this idea based on a uniform distribution of the intermediate temporal scale levels, we present a conceptual extension of this idea based on a logarithmic distribution of the intermediate temporal scale levels, and show that this leads to a family of kernels with different characteristics in that they correspond to more skewed distributions with the degree of skewness determined by a distribution parameter c .

In section 4 we analyse the temporal characteristics of these kernels and show that they lead to faster temporal characteristics in terms of shorter temporal delays, including how the choice of distribution parameter c affects these characteristics. In section 5 we present a more detailed analysis of these kernels, with emphasis on the limit case when the number of intermediate scale levels K tends to infinity, and making constructions that lead to true self-similarity and scale invariance over a discrete set of temporal scaling factors.

Section 6 shows how these spatial and temporal kernels can be transferred to a discrete implementation while preserving scale-space properties also in the discrete implementation and allowing for efficient computations of spatio-temporal derivative approximations. Section 7 develops a model for defining scale-normalized derivatives for the proposed temporal scale-space kernels, which also leads to a way of measuring how far from the time-causal limit kernel a particular temporal scale-space kernel is when using a finite number K of temporal scale levels.

In section 8 we combine these components for computing spatio-temporal features defined from different types of spatio-temporal differential invariants, including an analysis of their invariance or covariance properties under natural image transformations, with specific emphasis on independent scalings of the spatial and temporal dimensions, illumination variations and variations in exposure control mechanisms. Finally, section 9 concludes with a summary and discussion, including a description about relations and differences to other temporal scale-space models.

To simplify the presentation, we have put some of the theoretical analysis in the

appendix. Appendix A presents a frequency analysis of the proposed time-causal scale-space kernels, including a detailed characterization of the limit case when the number of temporal scale levels K tends to infinity and explicit expressions their moment (cumulant) descriptors up to order four. Appendix B presents a comparison with the temporal kernels in Koenderink’s scale-time model, including a minor modification of Koenderink’s model to make the temporal kernels normalized to unit L_1 -norm and a mapping between the parameters in his model (a temporal offset δ and a dimensionless amount of smoothing σ relative to a the logarithmic time scale) and the parameters in our model (a temporal variance τ , the distribution parameter c and the number of temporal scale levels K) including graphs of the similarities *vs.* differences between these two models.

2 Spatio-temporal receptive fields

The theoretical structure that we start from is a general result from axiomatic derivations of a spatio-temporal scale-space based on assumptions of non-enhancement of local extrema and the existence of a continuous temporal scale parameter, which states that the spatio-temporal receptive fields should be based on spatio-temporal smoothing kernels of the form (see overviews in Lindeberg [51, 52]):

$$T(x_1, x_2, t; s, \tau, v, \Sigma) = g(x_1 - v_1 t, x_2 - v_2 t; s, \Sigma) h(t; \tau) \quad (1)$$

where

- $x = (x_1, x_2)^T$ denotes the image coordinates,
- t denotes time,
- s denotes the spatial scale,
- τ denotes the temporal scale,
- $v = (v_1, v_2)^T$ denotes a local image velocity,
- Σ denotes a spatial covariance matrix determining the spatial shape of an affine Gaussian kernel $g(x; s, \Sigma) = \frac{1}{2\pi s \sqrt{\det \Sigma}} e^{-x^T \Sigma^{-1} x / 2s}$,
- $g(x_1 - v_1 t, x_2 - v_2 t; s, \Sigma)$ denotes a spatial affine Gaussian kernel that moves with image velocity $v = (v_1, v_2)$ in space-time and
- $h(t; \tau)$ is a temporal smoothing kernel over time.

For simplicity, we shall here restrict the family of affine Gaussian kernels over the spatial domain to rotationally symmetric Gaussians of different size s , by setting the covariance matrix Σ to a unit matrix. We shall also mainly restrict ourselves to space-time separable receptive fields by setting the image velocity v to zero.

A conceptual difference that we shall pursue is by relaxing the requirement of a continuous temporal scale parameter in the above axiomatic derivations by a discrete temporal scale parameter. We shall also replace the previous axiom about non-creation of new image structures with increasing scale in terms of non-enhancement of local extrema (which requires a continuous scale parameter) by the requirement that the temporal smoothing process, when seen as an operation along a one-dimensional temporal axis only, must not increase the number of local extrema or zero-crossings

in the signal. Then, another family of time-causal scale-space kernels becomes permissible and uniquely determined, in terms of first-order integrators or truncated exponential filters coupled in cascade.

The main topics of this paper are to handle the remaining degrees of freedom resulting from this construction about: (i) choosing and parameterizing the distribution of temporal scale levels, (ii) analysing the resulting temporal dynamics, (iii) describing how this model can be transferred to a discrete implementation while retaining discrete scale-space properties and (iv) using the resulting theoretical model for computing scale-normalized spatio-temporal derivative expressions for purposes in computer vision and (v) computational modelling of biological vision.

3 Time-causal temporal scale-space

When constructing a system for real-time processing of sensory data, a fundamental constraint on the temporal smoothing kernels is that they have to be *time-causal*. The ad hoc solution of using a truncated symmetric filter of finite temporal extent in combination with a temporal delay is not appropriate in a time-critical context. Because of computational and memory efficiency, the computations should furthermore be based on a compact temporal buffer that contains sufficient information for representing the sensory information at multiple temporal scales and computing features therefrom. Corresponding requirements are necessary in computational modelling of biological perception.

3.1 Time-causal scale-space kernels for pure temporal domain

To model the temporal component of the smoothing operation in equation (1), let us initially consider a signal $f(t)$ defined over a one-dimensional continuous temporal axis $t \in \mathbb{R}$. To define a one-parameter family of temporal scale-space representation from this signal, we consider a one-parameter family of smoothing kernels $h(t; \tau)$ where $\tau \geq 0$ is the temporal scale parameter

$$L(t; \tau) = h(t; \tau) * f(t) = \int_{u=0}^{\infty} h(u; \tau) f(t-u) du \quad (2)$$

and $L(t; 0) = f(t)$. To formalize the requirement that this transformation must not introduce new structures from a finer to a coarser temporal scale, let us following Lindeberg [40] require that between any pair of temporal scale levels $\tau_2 > \tau_1 \geq 0$ the number of local extrema at scale τ_2 must not exceed the number of local extrema at scale τ_1 . Let us additionally require the family of temporal smoothing kernels $h(u; \tau)$ to obey a cascade relation of the following form

$$h(t; \tau_2) = (\Delta h)(t; \tau_1 \mapsto \tau_2) * h(t; \tau_1) \quad (3)$$

between any pair of temporal scale levels (τ_1, τ_2) such that $\tau_2 > \tau_1$ for some family of transformation kernels $(\Delta h)(t; \tau_1 \mapsto \tau_2)$. Note that in contrast to most other axiomatic scale-space definitions, we do, however, not impose a strict semi-group property on the kernels. The motivation for this is to make it possible to take larger scale steps at coarser temporal scales, which will give higher flexibility and enable the construction of more efficient temporal scale-space representations.

Following Lindeberg [40], let us further define a scale-space kernel as a kernel that guarantees that the number of local extrema in the convolved signal can never exceed

the number of local extrema in the input signal. Equivalently, this condition can be expressed in terms of the number of zero-crossings in the signal. Following Lindeberg and Fagerström [58], let us additionally define a *temporal scale-space kernel* as a scale-space kernel that additionally satisfies the causality requirement $h(t; \tau) = 0$ if $t < 0$. If both the raw transformation kernels $h(u; \tau)$ and the cascade kernels $(\Delta h)(t; \tau_1 \mapsto \tau_2)$ are scale-space kernels, we do hence guarantee that the number of local extrema in $L(t; \tau_2)$ can never exceed the number of local extrema in $L(t; \tau_1)$. If the kernels $h(u; \tau)$ and additionally the cascade kernels $(\Delta h)(t; \tau_1 \mapsto \tau_2)$ are temporal scale-space kernels, these kernels do hence constitute natural kernels for defining a temporal scale-space representation.

3.2 Classification of scale-space kernels for continuous signals

Interestingly, the classes of scale-space kernels and temporal scale-space kernels can be completely classified based on classical results by Schoenberg and Karlin regarding the theory of variation-diminishing linear transformations. Schoenberg studied this topic in a series of papers over about 20 years (Schoenberg [66, 67, 68, 69, 70, 71]) and Karlin [33] then wrote an excellent monograph on the topic of total positivity.

Variation diminishing linear transformations. Summarizing main results from this theory on a form relevant to the construction of scale-space concept for one-dimensional signals (Lindeberg [43, section 3.5.1]), let $S^-(f)$ denotes the number of sign changes in a function f defined by

$$S^-(f) = \sup V^-(f(t_1), f(t_2), \dots, f(t_m)), \quad (4)$$

where the supremum is extended over all sets $t_1 < t_2 < \dots < t_J$ ($t_j \in \mathbb{R}$), J is arbitrary but finite, and $V^-(v)$ denotes the number of sign changes in a vector v . Then, the transformation

$$f_{out}(\eta) = \int_{\xi=-\infty}^{\infty} f_{in}(\eta - \xi) dG(\xi), \quad (5)$$

where G is a distribution function (essentially the primitive function of a convolution kernel), is said to be *variation-diminishing* if

$$S^-(f_{out}) \leq S^-(f_{in}) \quad (6)$$

holds for all continuous and bounded f_{in} . Specifically, the transformation (5) is variation diminishing if and only if G has a bilateral Laplace-Stieltjes transform of the form (Schoenberg [70])

$$\int_{\xi=-\infty}^{\infty} e^{-s\xi} dG(\xi) = C e^{\gamma s^2 + \delta s} \prod_{i=1}^{\infty} \frac{e^{a_i s}}{1 + a_i s} \quad (-c < \text{Re}(s) < c) \quad (7)$$

for some $c > 0$, where $C \neq 0$, $\gamma \geq 0$, δ and a_i are real, and $\sum_{i=1}^{\infty} a_i^2$ is convergent.

Classes of continuous scale-space kernels. Interpreted in the temporal domain, this result implies that for continuous signals there are four primitive types of linear and shift-invariant smoothing transformations; convolution with the *Gaussian kernel*,

$$h(\xi) = e^{-\gamma \xi^2}, \quad (8)$$

convolution with the *truncated exponential functions*,

$$h(\xi) = \begin{cases} e^{-|\lambda|\xi} & \xi \geq 0, \\ 0 & \xi < 0, \end{cases} \quad h(\xi) = \begin{cases} e^{|\lambda|\xi} & \xi \leq 0, \\ 0 & \xi > 0, \end{cases} \quad (9)$$

as well as trivial *translation* and *rescaling*. Moreover, it means that a shift-invariant linear transformation is a smoothing operation if and only if it can be decomposed into these primitive operations.

3.3 Temporal scale-space kernels over continuous temporal domain

In the above expressions, the first class of scale-space kernels (8) corresponds to using a non-causal Gaussian scale-space concept over time, which may constitute a straightforward model for analysing pre-recorded temporal data in an offline setting where temporal causality is not critical and can be disregarded by the possibility of accessing the virtual future in relation to any pre-recorded time moment.

Adding temporal causality as a necessary requirement, and with additional normalization of the kernels to unit L_1 -norm to leave a constant signal unchanged, it follows that the following family of truncated exponential kernels

$$h_{exp}(t; \mu_k) = \begin{cases} \frac{1}{\mu_k} e^{-t/\mu_k} & t \geq 0 \\ 0 & t < 0 \end{cases} \quad (10)$$

constitutes the only class of time-causal scale-space kernels over a continuous temporal domain in the sense of guaranteeing both temporal causality and non-creation of new local extrema (or equivalently zero-crossings) with increasing scale (Lindeberg [40]; Lindeberg and Fagerström [58]). The Laplace transform of such a kernel is given by

$$H_{exp}(q; \mu_k) = \int_{t=-\infty}^{\infty} h_{exp}(t; \mu_k) e^{-qt} dt = \frac{1}{1 + \mu_k q} \quad (11)$$

and coupling K such kernels in cascade leads to a composed filter

$$h_{composed}(t; \mu) = *_{k=1}^K h_{exp}(t; \mu_k) \quad (12)$$

having a Laplace transform of the form

$$H_{composed}(q; \mu) = \int_{t=-\infty}^{\infty} (*_{k=1}^K h_{exp}(t; \mu_k)) e^{-qt} dt = \prod_{k=1}^K \frac{1}{1 + \mu_k q}. \quad (13)$$

The composed filter has temporal mean and variance

$$m_K = \sum_{k=1}^K \mu_k \quad \tau_K = \sum_{k=1}^K \mu_k^2. \quad (14)$$

In terms of physical models, repeated convolution with such kernels corresponds to coupling a series of *first-order integrators* with time constants μ_k in cascade

$$\partial_t L(t; \tau_k) = \frac{1}{\mu_k} (L(t; \tau_{k-1}) - L(t; \tau_k)) \quad (15)$$

with $L(t; 0) = f(t)$. In the sense of guaranteeing non-creation of new local extrema or zero-crossings over time, these kernels have a desirable and well-founded smoothing

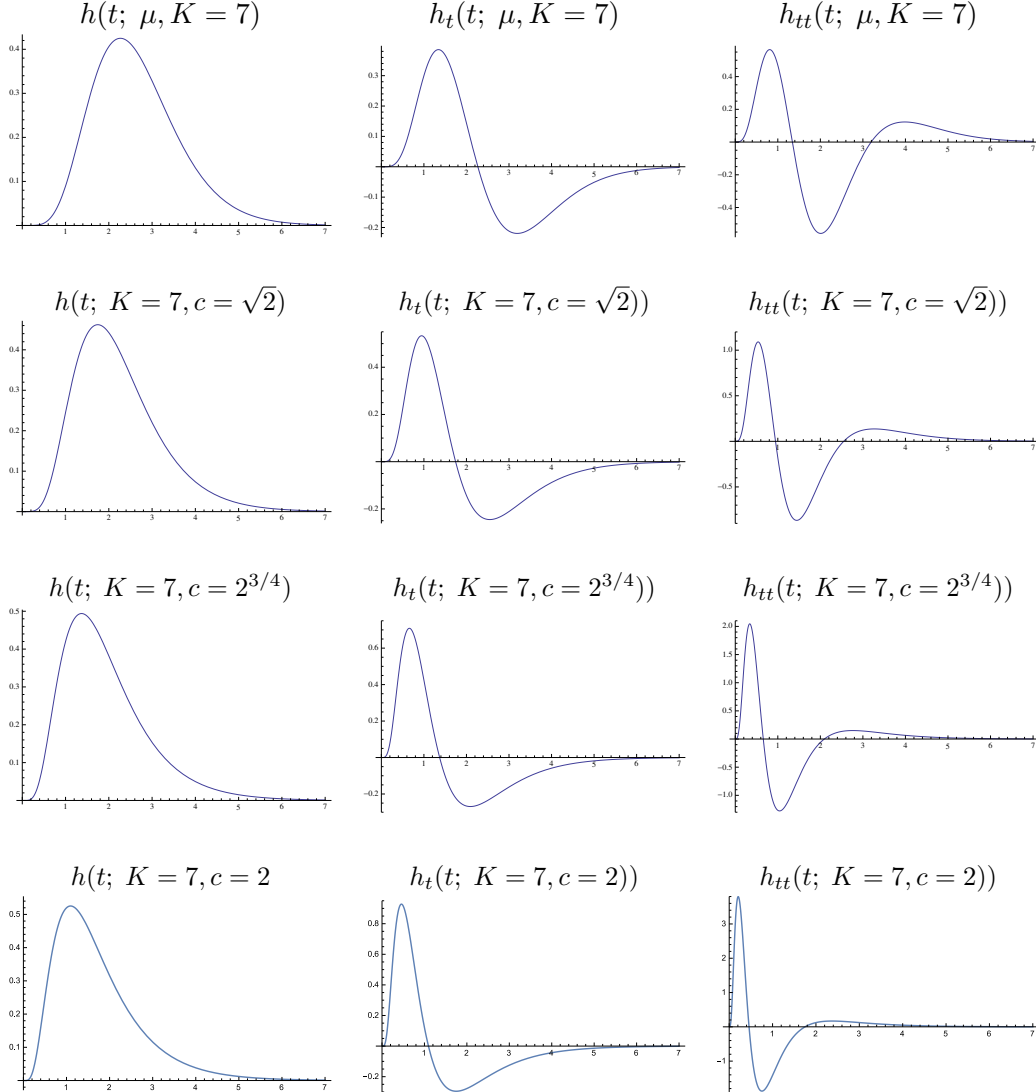


Figure 1: Equivalent kernels with temporal variance $\tau = 1$ corresponding to the composition of $K = 7$ truncated exponential kernels in cascade and their first- and second-order derivatives. (top row) Equal time constants μ . (second row) Logarithmic distribution of the scale levels for $c = \sqrt{2}$. (third row) Logarithmic distribution for $c = 2^{3/4}$. (bottom row) Logarithmic distribution for $c = 2$.

property that can be used for defining multi-scale observations over time. A constraint on this type of temporal scale-space representation, however, is that the *scale levels are required to be discrete* and that the scale-space representation does hence not admit a continuous scale parameter. Computationally, however, the scale-space representation based on truncated exponential kernels can be highly efficient and admits for direct implementation in terms of hardware (or wetware) that emulates first-order integration over time, and where the temporal scale levels together also serve as a sufficient time-recursive memory of the past (see figure 2).

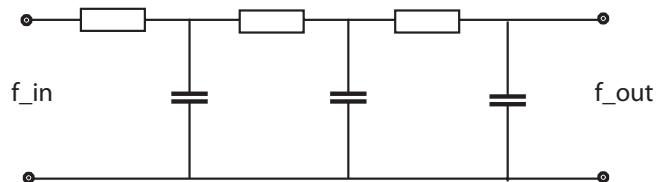


Figure 2: Electric wiring diagram consisting of a set of resistors and capacitors that emulate a series of first-order integrators coupled in cascade, if we regard the time-varying voltage f_{in} as representing the time varying input signal and the resulting output voltage f_{out} as representing the time varying output signal at a coarser temporal scale. According to the presented theory, the corresponding truncated exponential kernels of time are the only primitive temporal smoothing kernels that guarantee both temporal causality and non-creation of local extrema (alternatively zero-crossings) with increasing temporal scale. Such first-order temporal integration can be used as a straightforward computational model for temporal processing in biological neurons (see also Koch [34, Chapters 11–12] regarding physical modelling of the information transfer in dendrites of neurons).

Distributions of the temporal scale levels. When implementing this temporal scale-space concept, a set of intermediate scale levels τ_k has to be distributed between some minimum and maximum scale levels $\tau_{min} = \tau_1$ and $\tau_{max} = \tau_K$. Assuming that a total number of K scale levels is to be used, it is natural to distribute the temporal scale levels according to a geometric series, corresponding to a uniform distribution in units of effective temporal scale $\tau_{eff} = \log \tau$ (Lindeberg [42]). Using such a logarithmic distribution of the temporal scale levels, the different levels in the temporal scale-space representation at increasing temporal scales will serve as a logarithmic memory of the past, with qualitative similarity to the mapping of the past onto a logarithmic time axis in the scale-time model by Koenderink [36]. If we have the freedom of choosing τ_{min} freely, a natural way of parameterizing these temporal scale levels using a distribution parameter $c > 1$

$$\tau_k = c^{2(k-K)}\tau_{max} \quad (1 \leq k \leq K) \quad (16)$$

which by equation (14) implies that time constants of the individual first-order integrators will be given by

$$\mu_1 = c^{1-K}\sqrt{\tau_{max}} \quad (17)$$

$$\mu_k = \sqrt{\tau_k - \tau_{k-1}} = c^{k-K-1}\sqrt{c^2 - 1}\sqrt{\tau_{max}} \quad (2 \leq k \leq K) \quad (18)$$

If the temporal signal is on the other hand given at some minimum temporal scale level τ_{min} , we can instead determine $c = \left(\frac{\tau_{max}}{\tau_{min}}\right)^{\frac{1}{2(K-1)}}$ in (16) such that $\tau_1 = \tau_{min}$

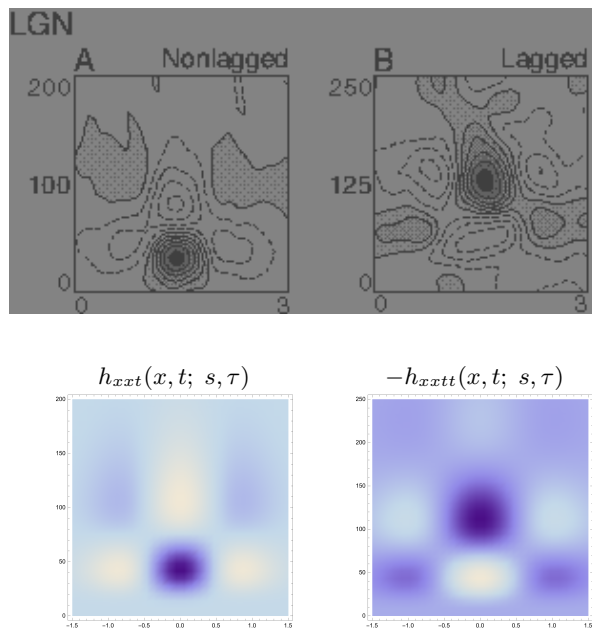


Figure 3: Computational modelling of space-time separable receptive field profiles in the lateral geniculate nucleus (LGN) as reported by DeAngelis *et al.* [9] using idealized spatio-temporal receptive fields of the form $T(x, t; s, \tau) = \partial_{x^\alpha} \partial_{t^\beta} g(; s) h(t; \tau)$ according to equation (1) and with the temporal smoothing function $h(t; \tau)$ modelled as a cascade of first-order integrators/truncated exponential kernels of the form (12). (left) a “non-lagged cell”, for which the first temporal lobe dominates, and modelled by first-order temporal derivatives (right) a “lagged cell”, for which the the second temporal lobe is strongest, and modelled in terms of second-order temporal derivatives. Parameter values: (a) h_{xxt} : $\sigma_x = 0.5$ degrees, $\sigma_t = 40$ ms. (b) h_{xxtt} : $\sigma_x = 0.6$ degrees, $\sigma_t = 60$ ms. (Horizontal dimension: space x . Vertical dimension: time t .)

and add $K - 1$ temporal scales with μ_k according to (18). Alternatively, if one chooses a uniform distribution of the intermediate temporal scale levels

$$\tau_k = \frac{k}{K} \tau_{max} \quad (19)$$

then the time constants are given by

$$\mu_k = \sqrt{\frac{\tau_{max}}{K}}. \quad (20)$$

3.4 Temporal receptive fields

Figure 1 shows graphs of such temporal scale-space kernels that correspond to the same value of the composed variance, using either a uniform distribution or a logarithmic distribution of the intermediate scale levels.

In general, these kernels are all highly asymmetric for small values of K , whereas the kernels based on a uniform distribution of the intermediate temporal scale levels become gradually more symmetric around the temporal maximum as K increases. The degree of continuity at the origin and the smoothness of transition phenomena increase with K such that coupling of $K \geq 2$ kernels in cascade implies a C^{K-2} -continuity of the temporal scale-space kernel. Specifically, the kernels based on a logarithmic distribution of the intermediate scale levels (i) have a higher degree of

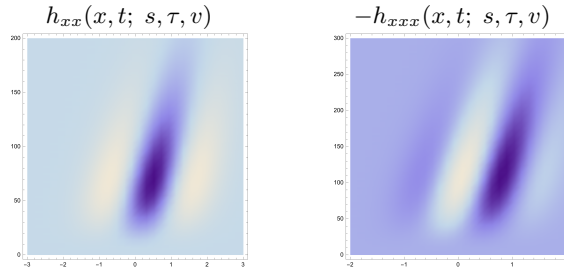
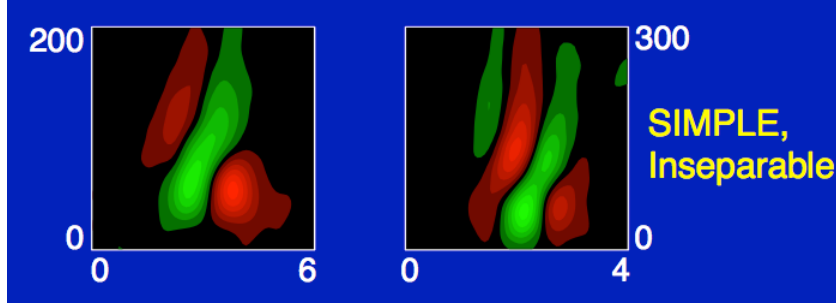
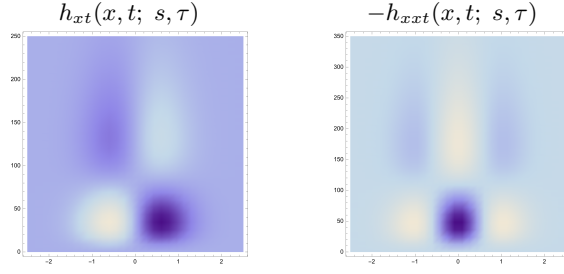
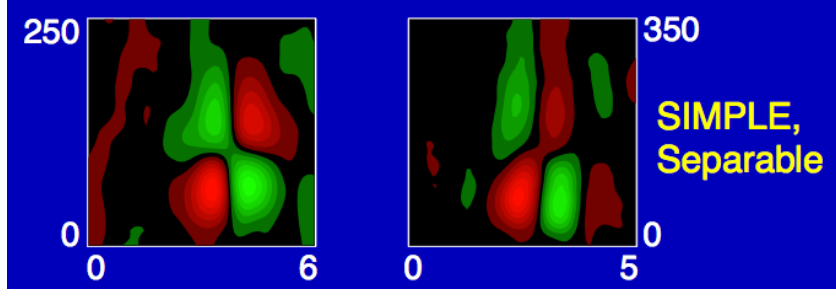


Figure 4: Computational modelling of simple cells in the primary visual cortex (V1) as reported by DeAngelis et al. [9] using idealized spatio-temporal receptive fields of the form $T(x, t; s, \tau, v) = \partial_{x^\alpha} \partial_{t^\beta} g(x - vt; s) h(t; \tau)$ according to equation (1) and with the temporal smoothing function $h(t; \tau)$ modelled as a cascade of first-order integrators/truncated exponential kernels of the form (12). (left column) Separable receptive fields corresponding to mixed derivatives of first- or second-order derivatives over space with first-order derivatives over time. (right column) Inseparable velocity-adapted receptive fields corresponding to second- or third-order derivatives over space. Parameter values: (a) h_{xt} : $\sigma_x = 0.6$ degrees, $\sigma_t = 60$ ms. (b) h_{xxt} : $\sigma_x = 0.6$ degrees, $\sigma_t = 80$ ms. (c) h_{xx} : $\sigma_x = 0.7$ degrees, $\sigma_t = 50$ ms, $v = 0.007$ degrees/ms. (d) h_{xxx} : $\sigma_x = 0.5$ degrees, $\sigma_t = 80$ ms, $v = 0.004$ degrees/ms. (Horizontal axis: Space x in degrees of visual angle. Vertical axis: Time t in ms.)

temporal asymmetry which increases with the distribution parameter c and (ii) allow for faster temporal dynamics compared to the kernels based on a uniform distribution of the intermediate scale levels.

3.5 Computational modelling of biological receptive fields

Receptive fields in the LGN. Regarding visual receptive fields in the lateral geniculate nucleus (LGN), DeAngelis *et al.* [9, 8] report that most neurons (i) have approximately circular center-surround organization in the spatial domain and that (ii) most of the receptive fields are separable in space-time. There are two main classes of temporal responses for such cells: (i) a “non-lagged cell” is defined as a cell for which the first temporal lobe is the largest one (figure 3(left)), whereas (ii) a “lagged cell” is defined as a cell for which the second lobe dominates (figure 3(right)).

Such temporal response properties are typical for *first- and second-order temporal derivatives* of a time-causal temporal scale-space representation. For the first-order temporal derivative of a time-causal temporal scale-space kernel, the first peak is strongest, whereas the second peak may be the most dominant one for second-order temporal derivatives. The spatial response, on the other hand, shows a high similarity to a Laplacian of a Gaussian, leading to an idealized receptive field model of the form (Lindeberg [52, equation (108)])

$$h_{LGN}(x, y, t; s, \tau) = \pm(\partial_{xx} + \partial_{yy}) g(x, y; s) \partial_t^n h(t; \tau), \quad (21)$$

Figure 3 shows results of modelling separable receptive fields in the LGN in this way, using a cascade of first-order integrators/truncated exponential kernels of the form (12) for modelling the temporal smoothing function $h(t; \tau)$.

Receptive fields in V1. Concerning the neurons in the primary visual cortex (V1), DeAngelis *et al.* [9, 8] describe that their receptive fields are generally different from the receptive fields in the LGN in the sense that they are (i) oriented in the spatial domain and (ii) sensitive to specific stimulus velocities. Cells (iii) for which there are precisely localized “on” and “off” subregions with (iv) spatial summation within each subregion, (v) spatial antagonism between on- and off-subregions and (vi) whose visual responses to stationary or moving spots can be predicted from the spatial subregions are referred to as simple cells (Hubel and Wiesel [28, 29]). In Lindeberg [52], an idealized model of such receptive fields was proposed of the form

$$\begin{aligned} h_{simple-cell}(x_1, x_2, t; s, \tau, v, \Sigma) = & (\cos \varphi \partial_{x_1} + \sin \varphi \partial_{x_2})^{m_1} (\sin \varphi \partial_{x_1} - \cos \varphi \partial_{x_2})^{m_2} \\ & (v_1 \partial_{x_1} + v_2 \partial_{x_2} + \partial_t)^n \\ & g(x_1 - v_1 t, x_2 - v_2 t; s \Sigma) h(t; \tau) \end{aligned} \quad (22)$$

where

- $\partial_\varphi = \cos \varphi \partial_{x_1} + \sin \varphi \partial_{x_2}$ and $\partial_{\perp\varphi} = \sin \varphi \partial_{x_1} - \cos \varphi \partial_{x_2}$ denote spatial directional derivative operators in two orthogonal directions φ and $\perp\varphi$,
- $m_1 \geq 0$ and $m_2 \geq 0$ denote the orders of differentiation in the two orthogonal directions in the spatial domain with the overall spatial order of differentiation $m = m_1 + m_2$,
- $v_1 \partial_{x_1} + v_2 \partial_{x_2} + \partial_t$ denotes a velocity-adapted temporal derivative operator

and the meanings of the other symbols are similar as explained in connection with equation (1).

Figure 4 shows the result of modelling the spatio-temporal receptive fields of simple cells in V1 in this way, using the general idealized model of spatio-temporal receptive fields in equation (1) in combination with a temporal smoothing kernel obtained by coupling a set of first-order integrators/truncated exponential kernels in cascade. As can be seen from the figures, the proposed idealized receptive field models do well reproduce the qualitative shape of the neurophysiologically recorded biological receptive fields.

These results complement the general theoretical model for visual receptive fields in Lindeberg [52] by (i) temporal kernels that have better temporal dynamics than the time-causal semi-group derived in Lindeberg [51] by decreasing faster with time (decreasing exponentially instead of polynomially) and with (ii) explicit modelling results and a theory for choosing and parameterizing the intermediate discrete temporal scale levels in the time-causal model.

With regard to a possible biological implementation of this theory, the evolution properties of the presented scale-space models over scale and time are governed by diffusion and difference equations (see equations (23)–(24) in next section), which can be implemented by *operations over neighbourhoods* in combination with first-order integration over time. Hence, the computations can naturally be implemented in terms of *connections between different cells*. Diffusion equations are also used in mean field theory for approximating the computations that are performed by populations of neurons (Omurtag *et al.* [62]; Mattia and Guidice [60]; Faugeras *et al.* [15]).

By combination of the theoretical properties of these kernels regarding scale-space properties between receptive field responses at different spatial and temporal scales as well as their covariance properties under natural image transformations (described in more detail in next section), the proposed theory can be seen as a both theoretically well-founded and biologically plausible model for time-causal and time-recursive spatio-temporal receptive fields.

3.6 Theoretical properties of time-causal spatio-temporal scale-space

Under evolution of time and with increasing spatial scale, the corresponding time-causal spatio-temporal scale-space representation generated by convolution with kernels of the form (1) with specifically the temporal smoothing kernel $h(t; \tau)$ defined as a set of truncated exponential kernels/first-order integrators in cascade (12) obeys the following system of differential/difference equations

$$\partial_s L = \frac{1}{2} \nabla_x^T (\Sigma \nabla_x L), \quad (23)$$

$$\partial_t L = -v^T (\nabla_x L) - \frac{1}{\mu_k} \Delta_\tau L \quad (24)$$

where the difference operator Δ_τ over temporal scale is defined as

$$(\Delta_\tau L)(x, t; s, \tau_k; \Sigma, v) = L(x, t; s, \tau_k; \Sigma, v) - L(x, t; s, \tau_{k-1}; \Sigma, v) \quad (25)$$

Theoretically, the resulting spatio-temporal scale-space representation obeys similar scale-space properties over the *spatial domain* as the two other spatio-temporal scale-space models derived in Lindeberg [51, 52, 53] regarding (i) linearity over the spatial domain, (ii) shift invariance over space, (iii) semi-group and cascade properties over

spatial scales, (iv) self-similarity and scale covariance over spatial scales, (v) non-enhancement of local extrema with increasing spatial scale and (vi) closedness and covariance under affine transformations over the spatial domain if basing the spatial smoothing operation on the general family of affine Gaussian kernels. When using rotationally symmetric Gaussian kernels for smoothing, the corresponding spatio-temporal scale-space representation does instead obey (vii) rotational invariance.

Over the *temporal domain*, these kernels obey (viii) linearity over the temporal domain, (ix) shift invariance over the temporal domain, (x) temporal causality, (xi) cascade property over temporal scales, (xii) non-creation of local extrema for any purely temporal signal. If using a uniform distribution of the intermediate temporal scale levels, the spatio-temporal scale-space representation obeys a (xiii) semi-group property over discrete temporal scales. Due to the use of a finite number of discrete temporal scale levels, the corresponding spatio-temporal scale-space representation cannot however for general values of the time constants μ_k obey full self-similarity and scale covariance over temporal scales. Using a logarithmic distribution of the temporal scale levels and an additional limit case construction to the infinity, we will however show in section 5 that it is possible to achieve (xiv) self-similarity and scale covariance over temporal scales for a discrete set of temporal scaling transformations.

Over the *composed spatio-temporal domain*, these kernels obey (xv) positivity and (xvi) unit normalization in L_1 -norm. The spatio-temporal scale-space representation does also obey (xvii) closedness and covariance under Galilean transformations in space-time.

4 Temporal dynamics of the time-causal kernels

For the time-causal filters obtained by coupling truncated exponential kernels in cascade, there will be an inevitable temporal delay depending on the time constants μ_k of the individual filters. A straightforward way of estimating this delay is by using the additive property of mean values under convolution $m_K = \sum_{k=1}^K \mu_k$ according to (14). In the special case when all the time constants are equal $\mu_k = \sqrt{\tau/K}$, this measure is given by

$$m_{uni} = \sqrt{K\tau} \quad (26)$$

showing that the temporal delay increases if the temporal smoothing operation is divided into a larger number of smaller individual smoothing steps.

In the special case when the intermediate temporal scale levels are instead distributed logarithmically according to (16), with the individual time constants given by (17) and (18), this measure for the temporal delay is given by

$$m_{log} = \frac{c^{-K} \left(c^2 - \left(\sqrt{c^2 - 1} + 1 \right) c + \sqrt{c^2 - 1} c^K \right)}{c - 1} \sqrt{\tau} \quad (27)$$

with the limit value

$$m_{log-limit} = \lim_{K \rightarrow \infty} m_{log} = \sqrt{\frac{c+1}{c-1}} \sqrt{\tau} \quad (28)$$

when the number of filters tends to infinity.

By comparing equations (26)–(27), we can specifically note that with increasing number of intermediate temporal scale levels a logarithmic distribution of the intermediate scales implies shorter temporal delays than a uniform distribution of the intermediate scales.

Table 1 shows numerical values of these measures for different values of K and c . As can be seen, the logarithmic distribution of the intermediate scales allows for significantly faster temporal dynamics than a uniform distribution.

Temporal mean values of time-causal kernels				
K	m_{uni}	$m_{log}(c = \sqrt{2})$	$m_{log}(c = 2^{3/4})$	$m_{log}(c = 2)$
2	1.414	1.414	1.399	1.366
3	1.732	1.707	1.636	1.549
4	2.000	1.914	1.777	1.641
5	2.236	2.061	1.860	1.686
6	2.449	2.164	1.910	1.709
7	2.646	2.237	1.940	1.721
8	2.828	2.289	1.957	1.726

Table 1: Numerical values of the *temporal delay in terms of the temporal mean* $m = \sum_{k=1}^K \mu_k$ in units of $\sigma = \sqrt{\tau}$ for time-causal kernels obtained by coupling K truncated exponential kernels in cascade in the cases of a uniform distribution of the intermediate temporal scale levels $\tau_k = k\tau/K$ or a logarithmic distribution $\tau_k = c^{2(k-K)}\tau$ with $c > 1$.

Temporal delays from the maxima of time-causal kernels				
K	$t_{max,uni}$	$t_{max,log}(c = \sqrt{2})$	$t_{max,log}(c = 2^{3/4})$	$t_{max,log}(c = 2)$
2	0.707	0.707	0.688	0.640
3	1.154	1.122	1.027	0.909
4	1.500	1.385	1.199	1.014
5	1.789	1.556	1.289	1.060
6	2.041	1.669	1.340	1.083
7	2.268	1.745	1.370	1.095
8	2.475	1.797	1.388	1.100

Table 2: Numerical values for the *temporal delay of the local maximum* in units of $\sigma = \sqrt{\tau}$ for time-causal kernels obtained by coupling K truncated exponential kernels in cascade in the cases of a uniform distribution of the intermediate temporal scale levels $\tau_k = k\tau/K$ or a logarithmic distribution $\tau_k = c^{2(k-K)}\tau$ with $c > 1$.

Additional temporal characteristics. Because of the asymmetric tails of the time-causal temporal smoothing kernels, temporal delay estimation by the mean value may however lead to substantial overestimates compared to *e.g.* the position of the local maximum. To provide more precise characteristics in the case of a uniform distribution of the intermediate temporal scale levels, for which a compact closed form expression is available for the composed kernel

$$h_{composed}(t; \mu, K) = \frac{t^{K-1} e^{-t/\mu}}{\mu^K \Gamma(K)} \quad (29)$$

let us differentiate this function $\partial_t (h_{composed}(t; \mu, K)) = \frac{e^{-\frac{t}{\mu}} ((K-1)\mu - t) \left(\frac{t}{\mu}\right)^{K+1}}{t^3 \Gamma(K)}$ and solve for the positions of the local maximum

$$t_{max,uni} = (K-1)\mu = \frac{(K-1)}{\sqrt{K}}\sqrt{\tau}. \quad (30)$$

Table 2 shows numerical values for the position of the local maximum for both types of time-causal kernels. As can be seen from the data, the temporal response properties are significantly faster for a logarithmic distribution of the intermediate scale levels

compared to a uniform distribution and the difference increases rapidly with K . These temporal delay estimates are also significantly shorter than the temporal mean values, in particular for the logarithmic distribution.

If we consider a temporal event that occurs as a step function over time (*e.g.* a new object appearing in the field of view) and if the time of this event is estimated from the local maximum over time in the first-order temporal derivative response, then the temporal variation in the response over time will be given by the shape of the temporal smoothing kernel. The local maximum over time will occur at a time delay equal to the time at which the temporal kernel has its maximum over time. Thus, the position of the maximum over time of the temporal smoothing kernel is highly relevant for quantifying the temporal response dynamics.

5 The scale-invariant time-causal limit kernel

When using a logarithmic distribution of the intermediate scale levels (16), the time constants of the individual first-order integrators are given by (17) and (18). Thus, the explicit expression for the Fourier transform (11) is of the form

$$\hat{h}_{exp}(\omega; \tau, c, K) = \frac{1}{1 + i c^{1-K} \sqrt{\tau} \omega} \prod_{k=2}^K \frac{1}{1 + i c^{k-K-1} \sqrt{c^2 - 1} \sqrt{\tau} \omega} \quad (31)$$

Characterization in terms of temporal moments. Although the explicit expression for the composed time-causal kernel may be somewhat cumbersome to handle for any finite value of K , in appendix A.1 we show how one based on a Taylor expansion of the Fourier transform can derive compact closed-form moment or cumulant descriptors of these time-causal scale-space kernels. Specifically, the limit values of the first-order moment M_1 and the higher-order central moments up to order four are when the number of temporal scale levels K tends to infinity given by

$$\lim_{K \rightarrow \infty} M_1 = \sqrt{\frac{c+1}{c-1}} \sqrt{\tau} \quad (32)$$

$$\lim_{K \rightarrow \infty} M_2 = \tau \quad (33)$$

$$\lim_{K \rightarrow \infty} M_3 = \frac{2(c+1)\sqrt{c^2-1}\tau^{3/2}}{(c^2+c+1)} \quad (34)$$

$$\lim_{K \rightarrow \infty} M_4 = \frac{3(3c^2-1)\tau^2}{c^2+1} \quad (35)$$

and give a coarse characterization of the limit behaviour of these kernels essentially corresponding to the terms in a Taylor expansion of the Fourier transform up to order four. Following a similar methodology, explicit expressions for higher-order moment descriptors can also be derived in an analogous fashion, from the Taylor coefficients of higher order, if needed for special purposes.

In figure 9 in appendix A.1 we show graphs of the corresponding skewness and kurtosis measures as function of the distribution parameter c , showing that both these measures increase with the distribution parameter c . In figure 12 in appendix B we provide a comparison between the behaviour of this limit kernel and the temporal kernel in Koenderink's scale-time model showing that although the temporal kernels in these two models to a first approximation share qualitatively coarsely similar properties in terms of their overall shape (see figure 11 in appendix B), the temporal

kernels in these two models differ significantly in terms of their skewness and kurtosis measures.

The limit kernel. By letting the number of temporal scale levels K tend to infinity, we can define a limit kernel $\Psi(t; \tau, c)$ via the limit of the Fourier transform (31) according to (and with the indices relabelled to better fit the limit case)

$$\hat{\Psi}(t; \tau, c) = \lim_{K \rightarrow \infty} \hat{h}_{exp}(\omega; \tau, c, K) = \prod_{k=1}^{\infty} \frac{1}{1 + i c^{-k} \sqrt{c^2 - 1} \sqrt{\tau} \omega} \quad (36)$$

By treating this limit kernel as an object by itself, which will be well-defined because of the rapid convergence by the summation of variances according to a geometric series, interesting relations can be expressed between the temporal scale-space representations

$$L(t; \tau, c) = \int_{u=0}^{\infty} \Psi(u; \tau, c) f(t - u) du \quad (37)$$

obtained by convolution with this limit kernel.

Self-similar recurrence relation for the limit kernel over temporal scales. When distributing the temporal scale levels according to the logarithmic distribution (16), the temporal scale levels will be given by (for $k = K, K - 1, K - 2, \dots$)

$$\tau_k \in \left\{ \tau_{max}, \frac{\tau_{max}}{c^2}, \frac{\tau_{max}}{c^4}, \frac{\tau_{max}}{c^6}, \dots \right\} \quad (38)$$

with the individual time constants μ_k according to

$$\mu_k \in \left\{ \frac{\sqrt{c^2 - 1}}{c} \sqrt{\tau_{max}}, \frac{\sqrt{c^2 - 1}}{c^2} \sqrt{\tau_{max}}, \frac{\sqrt{c^2 - 1}}{c^3} \sqrt{\tau_{max}}, \dots \right\} \quad (39)$$

Thus, we can equivalently obtain the limit case of the temporal scale-space representation at temporal scale $\tau = \tau_{max}$ by convolving the limit case of the temporal scale-space representation at scale $\tau = \tau_{max}/c^2$ with a truncated exponential kernel having time constant $\mu = \frac{\sqrt{c^2 - 1}}{c} \sqrt{\tau_{max}}$, leading to a recurrence relation of the form

$$L(t; \tau, c) = h_{exp}(t; \frac{\sqrt{c^2 - 1}}{c} \sqrt{\tau}) * L(t; \frac{\tau}{c^2}, c) \quad (40)$$

For the underlying limit kernel, the corresponding recurrence relation thus becomes

$$\Psi(\omega; \tau, c) = h_{exp}(t; \frac{\sqrt{c^2 - 1}}{c} \sqrt{\tau}) * \Psi(\omega; \frac{\tau}{c^2}, c) \quad (41)$$

and in terms of its Fourier transform

$$\hat{\Psi}(\omega; \tau, c) = \frac{1}{1 + i \frac{\sqrt{c^2 - 1}}{c} \sqrt{\tau} \omega} \hat{\Psi}(\omega; \frac{\tau}{c^2}, c) \quad (42)$$

This property is also directly reflected in the limit form (36)

$$\begin{aligned} \hat{\Psi}(t; \tau, c) &= \frac{1}{1 + i \frac{\sqrt{c^2 - 1}}{c} \sqrt{\tau} \omega} \prod_{k=2}^{\infty} \frac{1}{1 + i c^{-k} \sqrt{c^2 - 1} \sqrt{\tau} \omega} \\ &= \frac{1}{1 + i \frac{\sqrt{c^2 - 1}}{c} \sqrt{\tau} \omega} \prod_{k=1}^{\infty} \frac{1}{1 + i c^{-k} \sqrt{c^2 - 1} \sqrt{\frac{\tau}{c^2}} \omega} \end{aligned} \quad (43)$$

Behaviour under temporal rescaling transformations. Consider next a temporal scaling transformation of the form

$$f'(t') = f(t) \quad \text{for} \quad t' = St \quad (44)$$

which in the Fourier domain is mapped to the inverse scaling transformation

$$\hat{f}'(\omega') = \hat{f}(\omega) \quad \text{for} \quad \omega' = \frac{\omega}{S} \quad (45)$$

From the Fourier transform of the limit kernel (36), we can directly observe that for any scale factor S it holds that

$$\hat{\Psi}\left(\frac{\omega}{S}; S^2\tau, c\right) = \hat{\Psi}(\omega; \tau, c) \quad (46)$$

In the temporal domain, the limit kernel transforms according to

$$\frac{1}{S}\Psi(St; S^2\tau, c) = \Psi(t; \tau, c) \quad (47)$$

If we for a given choice of distribution parameter c rescale the input signal f by a scaling factor $S = 1/c$ such that $t' = 1/c$, it then follows that the scale-space representation of f' at temporal scale $\tau' = \tau/c^2$

$$L'(t'; \frac{\tau}{c^2}, c) = \Psi(t'; \frac{\tau}{c^2}, c) * f'(t') \quad (48)$$

will be equal to the temporal scale-space representation of the original signal f at scale τ

$$L'(t'; \tau', c) = L(t; \tau, c) \quad (49)$$

Thereby, by a rescaling of the original signal by a scaling factor c , a rescaled copy of the temporal scale-space representation of the original signal can be found at the next lower discrete temporal scale relative to the temporal scale-space representation of the original signal. Applied recursively, this result implies that the temporal scale-space representation obtained by convolution with the limit kernel *obeys a closedness property under temporal rescaling factors $S = c^j$ ($j \in \mathbb{Z}$) that are integer powers of the distribution parameter c .*

Self-similarity and scale invariance of the limit kernel. Combining the recurrence relations of the limit kernel with its transformation property under scaling transformations, it follows that the limit kernel can be regarded as self-similar in the sense that (i) the scale-space representation at a coarser temporal scale (here τ) can be recursively computed from the scale-space representation at a finer temporal scale (here τ/c^2), (ii) the representation at the coarser temporal scale is derived from the input in a functionally similar way as the representation at the finer temporal scale, (iii) the limit kernel and its Fourier transform transform in a self-similar way (47) and (46) under scaling transformations.

Given a value of the distribution parameter c , we can thus rescale the input signal by arbitrary integer powers of this parameter as scaling factors $S = c^j$ ($j \in \mathbb{Z}$) and still be able to perfectly match the temporal scale-space representations obtained by convolutions with the limit kernel obtained for the same value of the distribution parameter. The choice¹ of what value of the parameter c to use in an actual implementation is a trade-off between the denser sampling of the temporal scales obtained

¹The choice of distribution parameter c can of course also be influenced by other factors determined by the application in which the temporal scale space representation is used. In the treatment in this paper, we have largely focused on values of c in the range $c \in [\sqrt{2}, 2]$, with the lower bound determined from the criterion that the value of the first time constant μ_1 should not exceed the value of the second time constant μ_2 , which may be a natural criterion when only using a rather low number of temporal scale levels.

for lower values of c and the faster temporal dynamics and faster convergence towards the limit case obtained for larger values of c .

Hence, although the proposed temporal scale-space representation is defined only for a discrete while formally infinite subset of scale levels $\tau_k = c^{2^j}\tau_0$ ($j \in \mathbb{Z}$), the limit kernel allows for perfect scale invariance over a restricted set of scaling factors $S = c^j$ ($j \in \mathbb{Z}$) that matches this specific set of scale levels. Based on this desirable and highly useful property, it is thus natural to refer to the limit kernel as *the scale invariant time-causal limit kernel*.

With regard to the task of approximating the scale invariant time-causal limit kernel by a time-causal kernels based on only a finite number K of temporal scale levels, we will later in section 7.4 develop an approach to quantify the amount of deviation from the limit kernel, which will then provide a way to quantify the minimum number of temporal scale levels that will be needed to approximate scale-normalized temporal derivatives up to a given accuracy in a specific application.

6 Computational implementation

The computational model for spatio-temporal receptive fields presented here is based on spatio-temporal image data that are assumed to be continuous over time. When implementing this model on sampled video data, the continuous theory must be transferred to discrete space and discrete time.

In this section we describe how the temporal and spatio-temporal receptive fields can be implemented in terms of corresponding discrete scale-space kernels that possess scale-space properties over discrete spatio-temporal domains.

6.1 Classification of scale-space kernels for discrete signals

In section 3.2, we described how the class of continuous scale-space kernels over a one-dimensional domain can be classified based on classical results by Schoenberg regarding the theory of variation-diminishing transformations as applied to the construction of discrete scale-space theory in Lindeberg [40] [43, section 3.3]. To later map the temporal smoothing operation to theoretically well-founded discrete scale-space kernels, we shall in this section describe corresponding classification result regarding scale-space kernels over a discrete temporal domain.

Variation diminishing linear transformations. Let $v = (v_1, v_2, \dots, v_n)$ be a vector of n real numbers and let $V^-(v)$ denote the (minimum) number of sign changes obtained in the sequence v_1, v_2, \dots, v_n if all zero terms are deleted. Then, based on a main result by Schoenberg [69] the convolution transformation

$$f_{out}(t) = \sum_{n=-\infty}^{\infty} c_n f_{in}(t-n) \quad (50)$$

is variation-diminishing i.e.

$$V^-(f_{out}) \leq V^-(f_{in}) \quad (51)$$

holds for all f_{in} if and only if the generating function of the sequence of filter coefficients $\varphi(z) = \sum_{n=-\infty}^{\infty} c_n z^n$ is of the form

$$\varphi(z) = c z^k e^{(q_1 z^{-1} + q_2 z)} \prod_{i=1}^{\infty} \frac{(1 + \alpha_i z)(1 + \delta_i z^{-1})}{(1 - \beta_i z)(1 - \gamma_i z^{-1})} \quad (52)$$

where $c > 0$, $k \in \mathbb{Z}$, $q_{-1}, q_1, \alpha_i, \beta_i, \gamma_i, \delta_i \geq 0$ and $\sum_{i=1}^{\infty} (\alpha_i + \beta_i + \gamma_i + \delta_i) < \infty$. Interpreted over the temporal domain, this means that besides trivial rescaling and translation, there are three basic classes of discrete smoothing transformations:

- two-point weighted average or generalized binomial smoothing

$$\begin{aligned} f_{out}(x) &= f_{in}(x) + \alpha_i f_{in}(x-1) \quad (\alpha_i \geq 0), \\ f_{out}(x) &= f_{in}(x) + \delta_i f_{in}(x+1) \quad (\delta_i \geq 0), \end{aligned} \quad (53)$$

- moving average or first-order recursive filtering

$$\begin{aligned} f_{out}(x) &= f_{in}(x) + \beta_i f_{out}(x-1) \quad (0 \leq \beta_i < 1), \\ f_{out}(x) &= f_{in}(x) + \gamma_i f_{out}(x+1) \quad (0 \leq \gamma_i < 1), \end{aligned} \quad (54)$$

- infinitesimal smoothing or diffusion smoothing as arising from the continuous semi-groups made possible by the factor $e^{(q_{-1}z^{-1} + q_1z)}$.

To transfer the continuous first-order integrators derived in section 3.3 to a discrete implementation, we shall in this treatment focus on the first-order recursive filters, which by additional normalization constitute both the discrete correspondence and a numerical approximation of time-causal and time-recursive first-order temporal integration (15).²

6.2 Discrete temporal scale-space kernels based on recursive filters

Given video data that has been sampled by some temporal frame rate r , the temporal scale σ_t in the continuous model in units of seconds is first transformed to a variance τ relative to a unit time sampling

$$\tau = r^2 \sigma_t^2 \quad (55)$$

where r may typically be either 25 Hz or 50 Hz. Then, a discrete set of intermediate temporal scale levels τ_k is defined by (16) or (19) with the difference between successive scale levels according to $\Delta\tau_k = \tau_k - \tau_{k-1}$ (with $\tau_0 = 0$).

For implementing the temporal smoothing operation between two such adjacent scale levels (with the lower level in each pair of adjacent scales referred to as f_{in} and the upper level as f_{out}), we make use of a *first-order recursive filter* normalized to the form

$$f_{out}(t) - f_{out}(t-1) = \frac{1}{1 + \mu_k} (f_{in}(t) - f_{out}(t-1)) \quad (56)$$

²Concerning the other classes of discrete scale-space kernels permitted by this criterion, the special case when $q_{-1} = q_1$ of the diffusion smoothing corresponds to convolution with the (non-causal) discrete analogue of the Gaussian kernel that can be used for expressing separable smoothing operations over a spatial domain (61). Alternatively, if one requires the diffusion smoothing to be time-causal by setting q_{-1} to zero, then this factor can be shown to correspond to convolution with the time-causal Poisson kernel (Lindeberg and Fagerström [58]) which also corresponds to the limit case of recursive filters with equal time constants coupled in cascade when the scale increment tends to zero while the number of intermediate scale levels tends to infinity. Additionally, the case with discrete signals allows for smoothing with generalized binomial kernels, which can be made time-causal if combined with a suitable temporal delay. If using such time-delayed generalized binomial kernels for discrete temporal filtering, they may however lead to longer temporal delays and will in general require a larger temporal buffer of the past. They are therefore not time-recursive to the same extent as first-order recursive filters which do not require any additional buffer past information than the information contained in the temporal scale-space representations at different temporal scales themselves. These are the motivations for focusing on first-order recursive filters for discrete implementation of time-causal receptive fields.

and having a generating function of the form

$$H_{geom}(z) = \frac{1}{1 - \mu_k (z - 1)} \quad (57)$$

which is a time-causal kernel and satisfies discrete scale-space properties of guaranteeing that the number of local extrema or zero-crossings in the signal will not increase with increasing scale (Lindeberg [40]; Lindeberg and Fagerström [58]). Each such filter has temporal mean value $m_k = \mu_k$ and temporal variance $\Delta\tau_k = \mu_k^2 + \mu_k$, and we compute μ_k from $\Delta\tau_k$ according to

$$\mu_k = \frac{\sqrt{1 + 4\Delta\tau_k} - 1}{2}. \quad (58)$$

By the additive property of variances under convolution, the discrete variances of the discrete temporal scale-space kernels will perfectly match those of the continuous model, whereas the mean values and the temporal delays may differ somewhat. If the temporal scale τ_k is large relative to the temporal sampling density, the discrete model should be a good approximation in this respect.

By the time-recursive formulation of this temporal scale-space concept, the computations can be performed based on a compact temporal buffer over time, which contains the temporal scale-space representations at temporal scales τ_k and with no need for storing any additional temporal buffer of what has occurred in the past to perform the corresponding temporal operations.

Concerning the actual implementation of these operations computationally, it should be noted that on signal processing hardware or software with built-in support for higher order recursive filtering, if one is only interested in the receptive field response at a single temporal scale, then one can of course combine a set of K' first-order recursive filters (56) into a higher order recursive filter by multiplying their generating functions (57)

$$H_{composed}(z) = \prod_{k=1}^{K'} \frac{1}{1 - \mu_k (z - 1)} = \frac{1}{a_0 + a_1 z + a_2 z^2 + \dots + a_{K'} z^{K'}} \quad (59)$$

and performing K' recursive filtering steps by a single call to the signal processing hardware or software. If using such an approach, it should be noted that the composed call (??) may, however, not be as numerically well-conditioned as the individual smoothing steps, which are guaranteed to dampen any local perturbations and obey non-creation of new local extrema or equivalently zero-crossings. In our Matlab implementation for offline processing of this receptive field model, we have therefore delimited the number of compositions to $K' = 4$.

6.3 Discrete implementation of spatial Gaussian smoothing

To implement the spatial Gaussian operation on discrete sampled data, we do first transform a spatial scale parameter σ_x in units of *e.g.* degrees of visual angle to a spatial variance s relative to a unit sampling density according to

$$s = p^2 \sigma_x^2 \quad (60)$$

where p is the number of pixels per spatial unit *e.g.* in terms of degrees of visual angle at the image center. Then, we convolve the image data with the separable two-dimensional *discrete analogue of the Gaussian kernel* (Lindeberg [40])

$$T(n_1, n_2; s) = e^{-2s} I_{n_1}(s) I_{n_2}(s) \quad (61)$$

where I_n denotes the modified Bessel functions of integer order and which corresponds to the solution of the semi-discrete diffusion equation

$$\partial_s L(n_1, n_2; s) = \frac{1}{2}(\nabla_5^2 L)(n_1, n_2; s) \quad (62)$$

where ∇_{\times}^2 denotes the five-point discrete Laplacian operator defined by $(\nabla_5^2 f)(n_1, n_2) = f(n_1 - 1, n_2) + f(n_1 + 1, n_2) + f(n_1, n_2 - 1) + f(n_1, n_2 + 1) - 4f(n_1, n_2)$. These kernels constitute the natural way to define a scale-space concept for discrete signals corresponding to the Gaussian scale-space over a symmetric domain in the sense of guaranteeing non-enhancement of local extrema, while also ensuring a semi-group property $T(\cdot, \cdot; s_1) * T(\cdot, \cdot; s_2) = T(\cdot, \cdot; s_1 + s_2)$ over the discrete domain which implies that representations at coarser scales can be computed from representations at finer scales using a cascade property.

This operation can be implemented either by explicit spatial convolution with spatially truncated kernels $\sum_{n_1=-N}^N \sum_{n_2=-N}^N T(n_1, n_2; s) > 1 - \varepsilon$ for small ε of the order 10^{-8} to 10^{-6} with mirroring at the image boundaries (adiabatic boundary conditions corresponding to no heat transfer across the image boundaries) or using the closed-form expression of the Fourier transform

$$\varphi_T(\theta_1, \theta_2) = \sum_{n_1=-\infty}^{\infty} \sum_{n_2=-\infty}^{\infty} T(n_1, n_2; s) e^{-i(n_1\theta_1 + n_2\theta_2)} = e^{-2t(\sin^2(\frac{\theta_1}{2}) + \sin^2(\frac{\theta_2}{2}))} \quad (63)$$

Alternatively, to approximate rotational symmetry by higher degree of accuracy, one can define the 2-D spatial discrete scale-space from the solution of (Lindeberg [43, section 4.3])

$$\partial_s L = \frac{1}{2}((1 - \gamma)\nabla_5^2 L + \gamma\nabla_{\times 2}^2 L) \quad (64)$$

where $(\nabla_{\times 2}^2 f)(n_1, n_2) = \frac{1}{2}(f(n_1 + 1, n_2 + 1) + f(n_1 + 1, n_2 - 1) + f(n_1 - 1, n_2 + 1) + f(n_1 - 1, n_2 - 1) - 4f(n_1, n_2))$ and specifically the choice $\gamma = 1/3$ gives the best approximation of rotational symmetry. In practice, this operation can be implemented by first one step of diagonal separable discrete smoothing at scale $s_{\times} = s/3$ followed by a Cartesian separable discrete smoothing at scale $s_5 = 2s/3$ or using a closed form expression for the Fourier transform derived from the difference operators

$$\varphi_T(\theta_1, \theta_2) = e^{-(2-\gamma)t + (1-\gamma)(\cos \theta_1 + \cos \theta_2)t + (\gamma \cos \theta_1 \cos \theta_2)t} \quad (65)$$

6.4 Discrete implementation of spatio-temporal receptive fields

For separable spatio-temporal receptive fields, we implement the spatio-temporal smoothing operation by separable combination of the spatial and temporal scale-space concepts in sections 6.2 and 6.3. From this representation, spatio-temporal derivative approximations are then computed from *difference operators*

$$\delta_t = (-1, +1) \quad \delta_{tt} = (1, -2, 1) \quad (66)$$

$$\delta_x = (-\frac{1}{2}, 0, +\frac{1}{2}) \quad \delta_{xx} = (1, -2, 1) \quad (67)$$

expressed over the appropriate dimension. From the general theory in (Lindeberg [41]) it follows that the scale-space properties for the original zero-order signal will be transferred to such derivative approximations, thereby implying theoretically well-founded implementation of discrete derivative approximations.

For non-separable spatio-temporal receptive fields corresponding to a non-zero image velocity $v = (v_1, v_2)^T$, we implement the spatio-temporal smoothing operation by first warping the video data $(x'_1, x'_2)^T = (x_1 - v_1 t, x_2 - v_2 t)^T$ using spline interpolation. Then, we apply separable spatio-temporal smoothing in the transformed domain and unwarped the result back to the original domain. Over a continuous domain, such an operation is equivalent to convolution with corresponding velocity-adapted spatio-temporal receptive fields, while being significantly faster in a discrete implementation than corresponding explicit convolution with non-separable receptive fields over three dimensions.

In addition to a transfer of the scale-space properties from the continuous model to the discrete implementation, all the components in this discretization, the discrete Gaussian kernel, the time-recursive filters and the discrete derivative approximations, can be seen as mathematical approximations of the corresponding continuous counterparts. Thereby, the behaviour of the discrete implementation will approach the corresponding continuous model.

7 Scale normalization for spatio-temporal derivatives

When computing spatio-temporal derivatives at different scales, some mechanism is needed for normalizing the derivatives with respect to the spatial and temporal scales, to make derivatives at different spatial and temporal scales comparable and to enable spatial and temporal scale selection.

7.1 Scale normalization of spatial derivatives

For the Gaussian scale-space concept defined over a purely spatial domain, it can be shown that the canonical way of defining scale-normalized derivatives at different spatial scales s is according to (Lindeberg [49])

$$\partial_{\xi_1} = s^{\gamma_s/2} \partial_{x_1}, \quad \partial_{\xi_2} = s^{\gamma_s/2} \partial_{x_2}, \quad (68)$$

where γ_s is a free parameter. Specifically, it can be shown (Lindeberg [49, section 9.1]) that this notion of γ -normalized derivatives corresponds to normalizing the m :th order Gaussian derivatives $g_{\xi^m} = g_{\xi_1^{m_1} \xi_2^{m_2}}$ in N -dimensional image space to constant L_p -norms over scale

$$\|g_{\xi^m}(\cdot; s)\|_p = \left(\int_{x \in \mathbb{R}^N} |g_{\xi^m}(x; s)|^p dx \right)^{1/p} = G_{m, \gamma_s} \quad (69)$$

with

$$p = \frac{1}{1 + \frac{|m|}{N}(1 - \gamma_s)} \quad (70)$$

where the perfectly scale invariant case $\gamma_s = 1$ corresponds to L_1 -normalization for all orders $|m| = m_1 + \dots + m_N$. In this paper, we will throughout use this approach for normalizing spatial differentiation operators with respect to the spatial scale parameter s .

7.2 Scale normalization of temporal derivatives

If using a non-causal Gaussian scale-space concept over the temporal domain, it is straightforward to use a corresponding scale normalization approach for normalizing

temporal derivative operators with respect to the temporal scale

$$\partial_\zeta = \tau^{\gamma_\tau/2} \partial_t \quad (71)$$

while noting that different values of γ_τ could be preferable when performing scale selection over the temporal domain relative to the spatial domain, because of the different dimensionality of the spatial domain (2-D) compared to the temporal domain (1-D). For example, if we would like the selected scale from local maxima over scale of a second-order derivative operator applied to a 1-D Gaussian blob over the temporal domain to exactly match the variance of the blob, then one should choose $\gamma_\tau = 3/4$, whereas if one would like the selected scale from local extrema over scale of second-order derivative operators over a 2-D spatial domain to be equal to the scale of the blob, then one should choose $\gamma_s = 1$ in the scale selection step (Lindeberg [49, 48, 54]).

For the non-causal temporal scale-space concept based on first-order temporal integrators coupled in cascade, we can also define a corresponding notion of scale-normalized temporal derivatives

$$\partial_{\zeta^n} = \tau^{n\gamma_\tau/2} \partial_{t^n} \quad (72)$$

which will be referred to as *variance-based normalization* reflecting the fact the parameter τ corresponds to variance of the composed temporal smoothing kernel. Alternatively, we can determine a temporal scale normalization factor $\alpha_{n,\gamma_\tau}(\tau)$

$$\partial_{\zeta^n} = \alpha_{n,\gamma_\tau}(\tau) \partial_{t^n} \quad (73)$$

such that the L_p -norm (with p determined as function of γ according to (70)) of the corresponding composed scale-normalized temporal derivative computation kernel $\alpha_{n,\gamma_\tau}(\tau) h_{t^n}$ equals the L_p -norm of some other reference kernel, where we here initially take the L_p -norm of the corresponding Gaussian derivative kernels

$$\|\alpha_{n,\gamma_\tau}(\tau) h_{t^n}(\cdot; \tau)\|_p = \alpha_{n,\gamma_\tau}(\tau) \|h_{t^n}(\cdot; \tau)\|_p = \|g_{\xi^n}(\cdot; \tau)\|_p = G_{n,\gamma_\tau}. \quad (74)$$

This latter approach will be referred to as *L_p -normalization*.³

Note that these two normalization approaches are both applicable for both (i) the time-causal scale-space concept over a continuous temporal domain based on truncated exponential filters coupled in cascade and for (ii) the time-causal scale-space concept over a discrete temporal domain based on first-order recursive filters coupled in cascade, with the only minor difference that the norm $\|h_{t^n}(\cdot; \tau)\|_p$ of the n :th order derivative of the temporal smoothing kernel in equation (74) should be interpreted as the continuous L_p -norm over a continuous temporal domain

$$\|h_{t^n}(\cdot; \tau)\|_p = \left(\int_{t=-\infty}^{\infty} |h_{t^n}(t; \tau)|^p dt \right)^{1/p} \quad (75)$$

or as the discrete l_p -norm over a discrete temporal domain

$$\|h_{t^n}(\cdot; \tau)\|_p = \left(\sum_{t=-\infty}^{\infty} |h_{t^n}(t; \tau)|^p \right)^{1/p}. \quad (76)$$

³Thereby, these definitions generalize the previously defined notions of L_p -normalization and variance-based normalization over pyramids in (Lindeberg and Bretzner [57]) to temporal scale-space representations.

7.3 Computation of temporal scale normalization factors

For computing the temporal scale normalization factors

$$\alpha_{n,\gamma\tau}(\tau) = \frac{\|g_{\xi^n}(\cdot; \tau)\|_p}{\|h_{t^n}(\cdot; \tau)\|_p} \quad (77)$$

in (73) for L_p -normalization as defined according to (74), we (i) compute the L_p -norms of the scale-normalized Gaussian derivatives, either from the closed-form expressions in the special case when $\gamma = 1$ implying $p = 1$

$$G_{1,1} = \int_{-\infty}^{\infty} |g_{\xi}(u; t)| du \Big|_{\gamma=1} = \sqrt{\frac{2}{\pi}} \approx 0.797885, \quad (78)$$

$$G_{2,1} = \int_{-\infty}^{\infty} |g_{\xi^2}(u; t)| du \Big|_{\gamma=1} = \sqrt{\frac{8}{\pi e}} \approx 0.967883, \quad (79)$$

$$G_{3,1} = \int_{-\infty}^{\infty} |g_{\xi^3}(u; t)| du \Big|_{\gamma=1} = \sqrt{\frac{2}{\pi}} \left(1 + \frac{4}{e^{3/2}}\right) \approx 1.51003, \quad (80)$$

$$\begin{aligned} G_{4,1} &= \int_{-\infty}^{\infty} |g_{\xi^4}(u; t)| du \Big|_{\gamma=1} \\ &= \frac{4\sqrt{3}}{e^{3/2+\sqrt{3/2}}\sqrt{\pi}} (\sqrt{3-\sqrt{6}}e^{\sqrt{6}} + \sqrt{3+\sqrt{6}}) \approx 2.8006. \end{aligned} \quad (81)$$

or by computing the integrals for values of $\gamma \neq 1$ by numerical integration. For computing the discrete l_p -norm of discrete temporal derivative approximations (76) for discrete implementation of temporal receptive fields, we first filter a discrete delta function by the corresponding cascade of first-order integrators to obtain the temporal smoothing kernel and then apply discrete derivative approximation operators to this kernel to obtain the corresponding equivalent temporal scale-space derivative kernel from which the discrete l_p -norm is computed by straightforward summation.

To illustrate how the choice of temporal scale normalization method may affect the results in a discrete implementation, tables 3–4 show examples of temporal scale normalization factors computed in these ways by either (i) variance-based normalization $\tau^{n/2}$ according to (72) or (ii) L_p -normalization $\alpha_{n,\gamma\tau}(\tau)$ according to (73)–(74) for different orders of temporal temporal differentiation n and at different temporal scales τ , relative to a unit temporal sampling density. As can be seen from these tables, the numerical values of the resulting scale normalization factors may differ substantially depending on the type of scale normalization method and the underlying number of first-order recursive filters that are coupled in cascade. Therefore, the choice of temporal scale normalization method warrants specific attention in applications where the relations between numerical values of temporal derivatives at different temporal scales may have critical influence.

Specifically, we can note that the temporal scale normalization factors based on L_p -normalization differ more from the scale normalization factors from variance-based normalization (i) in the case of a logarithmic distribution of the intermediate temporal scale levels compared to a uniform distribution, (ii) when the distribution parameter c increases within the family of temporal receptive fields based on a logarithmic distribution of the intermediate scale levels or (iii) a very low number of recursive filters are coupled in cascade. In all three cases, the resulting temporal smoothing kernels become more asymmetric and do hence therefore differ more from the

Temporal scale normalization factors for $n = 1$ at $\tau = 1$					
K	$\tau^{n/2}$	$\alpha_{n,\gamma_\tau}(\tau)$ (uni)	$\alpha_{n,\gamma_\tau}(\tau)$ ($c = \sqrt{2}$)	$\alpha_{n,\gamma_\tau}(\tau)$ ($c = 2^{3/4}$)	$\alpha_{n,\gamma_\tau}(\tau)$ ($c = 2$)
2	1.000	0.744	0.744	0.737	0.723
3	1.000	0.805	0.794	0.765	0.736
4	1.000	0.847	0.814	0.771	0.737
5	1.000	0.877	0.821	0.772	0.738
6	1.000	0.901	0.823	0.772	0.738
7	1.000	0.920	0.823	0.772	0.738
8	1.000	0.935	0.823	0.772	0.738

Temporal scale normalization factors for $n = 1$ at $\tau = 16$					
K	$\tau^{n/2}$	$\alpha_{n,\gamma_\tau}(\tau)$ (uni)	$\alpha_{n,\gamma_\tau}(\tau)$ ($c = \sqrt{2}$)	$\alpha_{n,\gamma_\tau}(\tau)$ ($c = 2^{3/4}$)	$\alpha_{n,\gamma_\tau}(\tau)$ ($c = 2$)
2	4.000	3.056	3.056	3.016	2.938
3	4.000	3.398	3.341	3.210	3.041
4	4.000	3.553	3.432	3.223	3.068
5	4.000	3.642	3.442	3.227	3.071
6	4.000	3.731	3.452	3.228	3.071
7	4.000	3.744	3.457	3.228	3.071
8	4.000	3.809	3.459	3.228	3.071

Temporal scale normalization factors for $n = 1$ at $\tau = 256$					
K	$\tau^{n/2}$	$\alpha_{n,\gamma_\tau}(\tau)$ (uni)	$\alpha_{n,\gamma_\tau}(\tau)$ ($c = \sqrt{2}$)	$\alpha_{n,\gamma_\tau}(\tau)$ ($c = 2^{3/4}$)	$\alpha_{n,\gamma_\tau}(\tau)$ ($c = 2$)
2	16.000	12.270	12.270	12.084	11.711
3	16.000	13.612	13.420	12.835	12.147
4	16.000	14.242	13.732	12.932	12.162
5	16.000	14.610	13.815	12.930	12.155
6	16.000	14.850	13.816	12.927	12.152
7	16.000	15.018	13.817	12.922	12.151
8	16.000	15.145	13.817	12.922	12.151

Table 3: Numerical values of *scale normalization factors for temporal derivatives*, for either variance-based normalization $\tau^{n/2}$ or L_p -normalization $\alpha_{n,\gamma_\tau}(\tau)$, for temporal derivatives of order $n = 1$ and at temporal scales $\tau = 1$ and $\tau = 16$ relative to a unit temporal sampling rate with $\Delta t = 1$ and with $\gamma_\tau = 1$, for time-causal kernels obtained by coupling K first-order recursive filters in cascade with either a uniform distribution of the intermediate scale levels $\tau_k = k/K\tau$ or a logarithmic distribution $\tau_k = c^{2(k-K)}\tau$ for $c = \sqrt{2}$, $c = 2^{3/4}$ and $c = 2$, respectively.

symmetric Gaussian model that underlies the definition of the variance-based scale normalization factor $\tau^{n/2}$.

On the other hand, we can note that with increasing values of K , the numerical values of the scale normalization factors converge much faster to their limit values when using a logarithmic distribution of the intermediate scale levels compared to using a uniform distribution. Depending on the value of the distribution parameter c , the scale normalization factors do reasonably well approach their limit values after $K = 4$ to $K = 8$ scale levels, whereas much larger values of K would be needed if using a uniform distribution. The convergence rate is also faster for larger values of c .

7.4 Measuring the deviation from the scale-invariant limit kernel

To quantify how good approximation that a time-causal kernel with a finite number of K scale levels is to the limit case when the number of scale levels K tends to

Temporal scale normalization factors for $n = 2$ at $\tau = 1$					
K	$\tau^{n/2}$	$\alpha_{n,\gamma_\tau}(\tau)$ (uni)	$\alpha_{n,\gamma_\tau}(\tau)$ ($c = \sqrt{2}$)	$\alpha_{n,\gamma_\tau}(\tau)$ ($c = 2^{3/4}$)	$\alpha_{n,\gamma_\tau}(\tau)$ ($c = 2$)
2	1.000	0.617	0.617	0.606	0.586
3	1.000	0.711	0.694	0.649	0.607
4	1.000	0.738	0.718	0.659	0.609
5	1.000	0.755	0.721	0.660	0.609
6	1.000	0.768	0.722	0.660	0.609
7	1.000	0.779	0.722	0.660	0.609
8	1.000	0.787	0.722	0.660	0.609

Temporal scale normalization factors for $n = 2$ at $\tau = 16$					
K	$\tau^{n/2}$	$\alpha_{n,\gamma_\tau}(\tau)$ (uni)	$\alpha_{n,\gamma_\tau}(\tau)$ ($c = \sqrt{2}$)	$\alpha_{n,\gamma_\tau}(\tau)$ ($c = 2^{3/4}$)	$\alpha_{n,\gamma_\tau}(\tau)$ ($c = 2$)
2	16.000	4.622	4.622	4.472	4.172
3	16.000	8.429	8.017	6.897	5.701
4	16.000	10.184	9.160	7.885	6.208
5	16.000	11.363	9.698	7.871	6.296
6	16.000	12.241	10.022	7.864	6.305
7	16.000	12.690	10.088	7.862	6.305
8	16.000	13.106	10.068	7.862	6.305

Temporal scale normalization factors for $n = 2$ at $\tau = 256$					
K	$\tau^{n/2}$	$\alpha_{n,\gamma_\tau}(\tau)$ (uni)	$\alpha_{n,\gamma_\tau}(\tau)$ ($c = \sqrt{2}$)	$\alpha_{n,\gamma_\tau}(\tau)$ ($c = 2^{3/4}$)	$\alpha_{n,\gamma_\tau}(\tau)$ ($c = 2$)
2	256.00	58.95	58.95	56.63	51.84
3	256.00	133.37	127.68	112.66	94.71
4	256.00	165.14	148.96	124.04	101.16
5	256.00	183.75	156.04	126.42	101.13
6	256.00	195.99	158.69	126.65	101.12
7	256.00	204.71	159.17	126.56	101.12
8	256.00	211.10	159.23	126.55	101.12

Table 4: Numerical values of *scale normalization factors for temporal derivatives*, for either variance-based normalization $\tau^{n/2}$ or L_p -normalization $\alpha_{n,\gamma_\tau}(\tau)$, for temporal derivatives of order $n = 2$ and at temporal scales $\tau = 1$ and $\tau = 16$ relative to a unit temporal sampling rate with $\Delta t = 1$ and with $\gamma_\tau = 1$, for time-causal kernels obtained by coupling K first-order recursive filters in cascade with either a uniform distribution of the intermediate scale levels $\tau_k = k/K\tau$ or a logarithmic distribution $\tau_k = c^{2(k-K)}\tau$ for $c = \sqrt{2}$, $c = 2^{3/4}$ and $c = 2$, respectively.

infinity, let us measure the relative deviation of the scale normalization factors from the limit case according to

$$\varepsilon_n(\tau) = \frac{|\alpha_n(\tau)|_K - \alpha_n(\tau)|_{K \rightarrow \infty}|}{\alpha_n(\tau)|_{K \rightarrow \infty}} \quad (82)$$

Table 5 shows numerical estimates of this relative deviation measure for different values of K from $K = 2$ to $K = 32$ for the time-causal kernels obtained from a uniform *vs.* a logarithmic distribution of the scale values. From the table, we can first of all note that the convergence rate with increasing values of K is significantly faster when using a logarithmic *vs.* a uniform distribution of the intermediate scale levels. Not even $K = 32$ scale levels is sufficient to drive the relative deviation measure below 1 % for a uniform distribution, whereas the corresponding deviation measures are down to machine precision when using $K = 32$ levels for a logarithmic distribution. When using $K = 4$ scale levels, the relative derivation measure is down

Relative deviation from limit of scale normalization factors for $n = 1$ at $\tau = 256$				
K	ε_n (uni)	ε_n ($c = \sqrt{2}$)	ε_n ($c = d^{3/4}$)	ε_n ($c = 2$)
2	0.233	$1.1 \cdot 10^{-1}$	$6.5 \cdot 10^{-2}$	$3.6 \cdot 10^{-2}$
4	0.110	$6.1 \cdot 10^{-3}$	$8.5 \cdot 10^{-4}$	$8.6 \cdot 10^{-4}$
8	0.053	$4.9 \cdot 10^{-4}$	$1.1 \cdot 10^{-5}$	$2.0 \cdot 10^{-7}$
16	0.026	$1.2 \cdot 10^{-7}$	$9.0 \cdot 10^{-13}$	$1.5 \cdot 10^{-15}$
32	0.013	$3.1 \cdot 10^{-14}$	$2.9 \cdot 10^{-14}$	$3.4 \cdot 10^{-14}$

Relative deviation from limit of scale normalization factors for $n = 2$ at $\tau = 256$				
K	ε_n (uni)	ε_n ($c = \sqrt{2}$)	ε_n ($c = d^{3/4}$)	ε_n ($c = 2$)
2	0.770	$6.3 \cdot 10^{-1}$	$5.5 \cdot 10^{-1}$	$4.9 \cdot 10^{-1}$
4	0.354	$6.5 \cdot 10^{-2}$	$2.0 \cdot 10^{-2}$	$4.1 \cdot 10^{-2}$
8	0.174	$3.2 \cdot 10^{-4}$	$1.3 \cdot 10^{-5}$	$1.6 \cdot 10^{-8}$
16	0.085	$1.8 \cdot 10^{-7}$	$1.0 \cdot 10^{-12}$	$9.6 \cdot 10^{-15}$
32	0.042	$1.2 \cdot 10^{-13}$	$6.2 \cdot 10^{-14}$	$4.0 \cdot 10^{-14}$

Table 5: Numerical estimates of the relative deviation from the limit case when using different numbers K of temporal scale levels for a uniform *vs.* a logarithmic distribution of the intermediate scale levels. The deviation measure ε_n according to equation (82) measures the relative deviation of the scale normalization factors when using a finite value K of temporal scale levels compared to the limit case when the number of temporal scale levels K tends to infinity. (These estimates have been computed at a coarse temporal scale $\tau = 256$ relative to a unit grid spacing so that the influence of discretization effects should be small. The limit case has been approximated by $K = 1000$ for the uniform distribution and $K = 500$ for the logarithmic distribution.)

to 10^{-2} to 10^{-4} for a logarithmic distribution. If using $K = 8$ scale levels, the relative deviation measure is down to 10^{-4} to 10^{-8} depending on the value of the distribution parameter c and the order n of differentiation.

From these results, we can conclude that one should not use a too low number of recursive filters that are coupled in cascade when computing temporal derivatives. Our recommendation is to use a logarithmic distribution with a minimum of four recursive filters for derivatives up to order two at finer scales and a larger number of recursive filters at coarser scales. When performing computations at a single temporal scale, we often use $K = 7$ as default.

8 Spatio-temporal feature detection

In the following, we shall apply the above theoretical framework for separable time-causal spatio-temporal receptive fields for computing different types of spatio-temporal feature, defined from spatio-temporal derivatives of different spatial and temporal orders, which may additionally be combined into composed (linear or non-linear) differential expressions.

8.1 Partial derivatives

A most basic approach is to first define a spatio-temporal scale-space representation $L: \mathbb{R}^2 \times \mathbb{R} \times \mathbb{R}_+ \times \mathbb{R}_+$ from any video data $f: \mathbb{R}^2 \times \mathbb{R}$ and then defining partial derivatives of any spatial and temporal orders $m = (m_1, m_2)$ and n at any spatial and temporal scales s and τ according to

$$L_{x_1^{m_1} x_2^{m_2} t^n}(x_1, x_2, t; s, \tau) = \partial_{x_1^{m_1} x_2^{m_2} t^n} (g(x_1, x_2; s) * h(t; \tau) * f(x_1, x_2, t)) \quad (83)$$

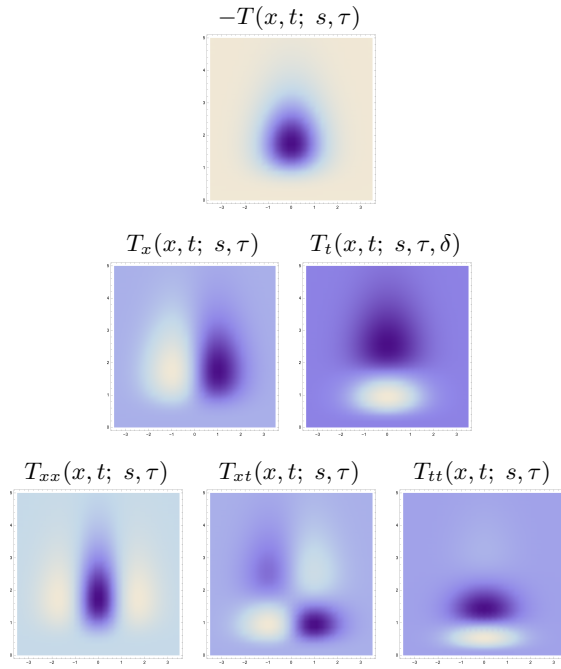


Figure 5: *Space-time separable kernels* $T_{x^m t^n}(x, t; s, \tau) = \partial_{x^m t^n}(g(x; s) * h(t; \tau))$ up to order two obtained as the composition of Gaussian kernels over the spatial domain x and a cascade of truncated exponential kernels over the temporal domain t with a logarithmic distribution of the intermediate temporal scale levels ($s = 1$, $\tau = 1$, $K = 7$, $c = \sqrt{2}$). (Horizontal axis: space x . Vertical axis: time t .)

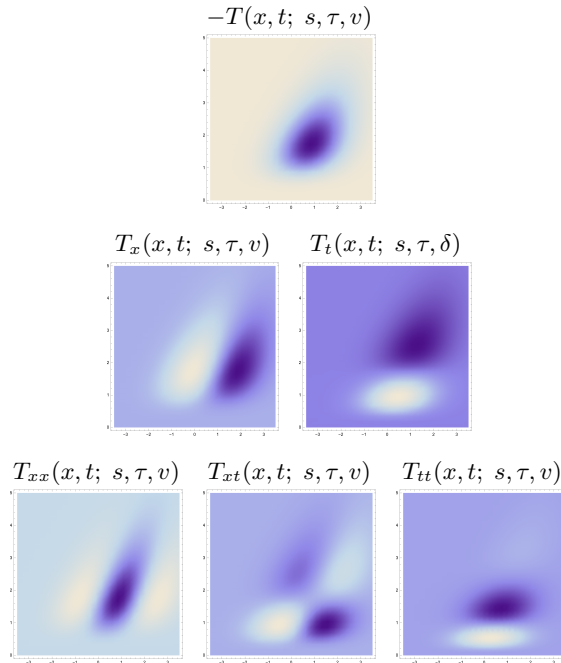


Figure 6: *Velocity-adapted spatio-temporal kernels* $T_{x^m t^n}(x, t; s, \tau, v) = \partial_{x^m t^n}(g(x - vt; s) * h(t; \tau))$ up to order two obtained as the composition of Gaussian kernels over the spatial domain x and a cascade of truncated exponential kernels over the temporal domain t with a logarithmic distribution of the intermediate temporal scale levels ($s = 1$, $\tau = 1$, $K = 7$, $c = \sqrt{2}$, $v = 0.5$). (Horizontal axis: space x . Vertical axis: time t .)

leading to a spatio-temporal N -jet representation of any order

$$\{L_x, L_y, L_t, L_{xx}, L_{xy}, L_{yy}, L_{xt}, L_{yt}, L_{tt}, \dots\} \quad (84)$$

here with intentionally somewhat sloppy notation for the convolution operation in equation (83) to simplify notation including interchangeable use of (x_1, x_2) or (x, y) for representing the spatial coordinates to simplify the formulation of spatio-temporal differential expressions in later equations. Figure 5 shows such kernels up to order two in the case of a 1+1-D space-time.

8.2 Directional derivatives

By linear combination of partial derivative operators, directional derivative operators can be expressed for any orientation φ in image space and any orthogonal direction $\perp\varphi$

$$\partial_\varphi = \cos \varphi \partial_x + \sin \varphi \partial_y \quad \partial_{\perp\varphi} = \sin \varphi \partial_x - \cos \varphi \partial_y. \quad (85)$$

and for any motion direction $v = (v_1, v_2, 1) = (v_x, v_y, 1)$ in space-time

$$\partial_{t_v} = \partial_t + v_x \partial_x + v_y \partial_y. \quad (86)$$

By combining such spatial and spatio-temporal directional derivative operators, filter bank responses can be created

$$L_{\varphi^{m_1} \perp\varphi^{m_2} t_v^n} = \partial_\varphi^{m_1} \partial_{\perp\varphi}^{m_2} \partial_{t_v}^n L \quad (87)$$

for different sampling strategies over image orientations φ and $\perp\varphi$ in image space and motion directions v in space-time (see figure 6 for illustrations of such kernels up to order two for a given velocity v in the case of a 1+1-D space-time).

Note that as long as the spatio-temporal smoothing operations are performed based on rotationally symmetric Gaussian kernels over the spatial domain and using space-time separable kernels over space-time, the responses to these directional derivative operators are can be directly related to corresponding partial derivative operators by mere linear combinations. If extending the rotationally symmetric Gaussian scale-space concept is extended to an anisotropic affine Gaussian scale-space and/or if we make use of non-separable velocity-adapted receptive fields over space-time in a spatio-temporal scale space, to enable true affine and/or Galilean invariances, such linear relationships will, however, no longer hold on a similar form.

For the image orientations φ and $\perp\varphi$, it is for purely spatial derivative operations in the case of rotationally symmetric smoothing over the spatial domain in principle sufficient to to sample the image orientation according to a uniform distribution on the semi-circle using at least $|m|+1$ directional derivative filters for directional derivatives of order $|m|$.

For temporal directional derivative operators to make fully sense in a geometrically meaningful manner (covariance under Galilean transformations in space-time), the directional derivative operation (86) should however also be combined with Galilean velocity adaptation of the spatio-temporal smoothing operation in a corresponding direction v according to (1). Regarding the distribution of such motion directions $v = (v_x, v_y)$, it is natural to distribute the magnitudes $|v| = \sqrt{v_x^2 + v_y^2}$ according to a self-similar distribution

$$|v|_j = |v|_1 \varrho^j \quad j = 1 \dots J \quad (88)$$

for some suitably selected constant $\varrho > 1$ and using a uniform distribution of the motion directions $e_v = v/|v|$ on the full circle.

8.3 Differential invariants over spatial derivative operators

Another most basic approach consists of applying the theory of spatial differential invariants in scale space (Florack et al [20, 21]; Lindeberg [43, 49, 48, 50]) to a spatio-temporal scale space representation, for computing differential expressions such as

$$|\nabla_{(x,y)}L| = \sqrt{L_x^2 + L_y^2} \quad (89)$$

$$\nabla_{(x,y)}^2 L = L_{xx} + L_{yy} \quad (90)$$

$$\det \mathcal{H}_{(x,y)}L = L_{xx}L_{yy} - L_{xy}^2 \quad (91)$$

$$\tilde{L}_{vv} = L_x^2 L_{xx} + 2L_x L_y L_{xy} + L_y^2 L_{yy} \quad (92)$$

$$L_{pp} = \frac{1}{2} \left(L_{xx} + L_{yy} - \sqrt{(L_{xx} - L_{yy})^2 + 4L_{xy}^2} \right) \quad (93)$$

$$L_{qq} = \frac{1}{2} \left(L_{xx} + L_{yy} + \sqrt{(L_{xx} - L_{yy})^2 + 4L_{xy}^2} \right) \quad (94)$$

$$\tilde{\kappa}(L) = L_x^2 L_{yy} + L_y^2 L_{xx} - 2L_x L_y L_{xy} \quad (95)$$

$$\mathcal{Q}_{(x,y)}L = L_x^2 + L_y^2 + C(L_{xx}^2 + 2L_{xy}^2 + L_{yy}^2) \quad (96)$$

These differential expressions are all invariant under rotations of the spatial image domain, in contrast to the partial derivatives $L_{x_1^{\alpha_1} x_2^{\alpha_2}}$, whose numerical values may depend strongly on the orientation of the object in the spatial image domain. In this list, the spatial gradient magnitude $|\nabla_{(x,y)}L|$ and the second-order derivative in the spatial gradient direction \tilde{L}_{vv} are used for edge detection; the spatial Laplacian $\nabla_{(x,y)}^2 L$, the determinant of the spatial Hessian $\det \mathcal{H}_{(x,y)}L$ and the rescaled curvature of level curves over the spatial domain $\tilde{\kappa}(L)$ can be used for interest point detection; the principal spatial curvatures of the image intensities L_{pp} and L_{qq} are used for ridge detection; while the quasi quadrature entity $\mathcal{Q}_{(x,y)}L$ is a measure of the amount of information in the first- and second-order spatial derivatives for which one can typically choose $C = 2/3$ or $C = e/4$ (Lindeberg [47]).

Scale-normalized spatial derivative expressions. Normalization of these entities with respect to the spatial scale parameter is then performed by replacing the spatial derivative operators ∂_x and ∂_y by the corresponding scale-normalized derivative operators

$$\partial_\xi = s^{\gamma/2} \partial_x, \quad \partial_\eta = s^{\gamma/2} \partial_y, \quad (97)$$

leading to the following scale-normalized differential expressions for $\gamma = 1$

$$|\nabla_{(x,y),norm}L| = \sqrt{sL_x^2 + sL_y^2} = \sqrt{s} |\nabla_{(x,y)}L| \quad (98)$$

$$\nabla_{(x,y),norm}^2 L = s(L_{xx} + L_{yy}) = s \nabla_{(x,y)}^2 L \quad (99)$$

$$\det \mathcal{H}_{(x,y),norm}L = s^2(L_{xx}L_{yy} - L_{xy}^2) = s^2 \det \mathcal{H}_{(x,y)}L \quad (100)$$

$$\tilde{L}_{vv,norm} = s^2(L_x^2 L_{xx} + 2L_x L_y L_{xy} + L_y^2 L_{yy}) = s^2 \tilde{L}_{vv} \quad (101)$$

$$L_{pp,norm} = \frac{s}{2} \left(L_{xx} + L_{yy} - \sqrt{(L_{xx} - L_{yy})^2 + 4L_{xy}^2} \right) = s L_{pp} \quad (102)$$

$$L_{qq,norm} = \frac{s}{2} \left(L_{xx} + L_{yy} + \sqrt{(L_{xx} - L_{yy})^2 + 4L_{xy}^2} \right) = s L_{qq} \quad (103)$$

$$\tilde{\kappa}_{norm}(L) = s^2(L_x^2 L_{yy} + L_y^2 L_{xx} - 2L_x L_y L_{xy}) = s^2 \tilde{\kappa}(L) \quad (104)$$

$$\mathcal{Q}_{(x,y),norm}L = s(L_x^2 + L_y^2) + C s^2(L_{xx}^2 + 2L_{xy}^2 + L_{yy}^2) \quad (105)$$

Note that by the homogeneity of the differential expressions for $|\nabla_{(x,y)}L|$, $\nabla_{(x,y)}^2L$, $\det \mathcal{H}_{(x,y)}$, \tilde{L}_{vv} , L_{pp} , L_{qq} and $\tilde{\kappa}(L)$ in terms of the order of differentiation and the number of different partial derivatives of different order that are multiplied together, the normalized differential expression $\mathcal{D}_{norm}L$ can be computed from the corresponding unnormalized differential expression $\mathcal{D}L$ by a mere multiplication

$$\mathcal{D}_{norm}L = s^{M\gamma/2} \mathcal{D}L \quad (106)$$

where $M = 1$ for $|\nabla_{(x,y)}L|$, $M = 2$ for $\nabla_{(x,y)}^2L$, $M = 4$ for $\det \mathcal{H}_{(x,y)}$, $M = 4$ for \tilde{L}_{vv} , $M = 2$ for L_{pp} and L_{qq} and $M = 4$ for $\tilde{\kappa}(L)$. The differential expression $\mathcal{Q}_{(x,y)}L$ does, however, differ by not being homogeneous in this respect, but can nevertheless lead to scale invariance, if adding derivatives of different orders into an inhomogeneous expression in the specific case of $\gamma = 1$.

8.4 Space-time coupled spatio-temporal derivative expressions

A more general approach to spatio-temporal feature detection consists of defining spatio-temporal derivative operators that combine spatial and temporal derivative operators in an integrated manner.

Temporal derivatives of the spatial Laplacian. Inspired by the way neurons in the lateral geniculate nucleus (LGN) respond to visual input (DeAngelis et al [9, 8]), which for many LGN cells can be modelled by idealized operations of the form (Lindeberg [52, equation (108)])

$$h_{LGN}(x, y, t; s, \tau) = \pm(\partial_{xx} + \partial_{yy})g(x, y; s) \partial_{t^n}h(t; \tau), \quad (107)$$

we can define the following differential entities

$$\partial_t(\nabla_{(x,y)}^2L) = L_{xxt} + L_{yyt} \quad (108)$$

$$\partial_{tt}(\nabla_{(x,y)}^2L) = L_{xxtt} + L_{yytt} \quad (109)$$

and combine these entities into a quasi quadrature measure over time of the form

$$\mathcal{Q}_t(\nabla_{(x,y)}^2L) = \left(\partial_t(\nabla_{(x,y)}^2L)\right)^2 + C \left(\partial_{tt}(\nabla_{(x,y)}^2L)\right)^2 \quad (110)$$

where C again may be set to $C = 2/3$ or $C = e/4$. The first entity $\partial_t(\nabla_{(x,y)}^2L)$ can be expected to give strong responses to spatial blob responses whose intensity values vary over time, whereas the second entity $\partial_{tt}(\nabla_{(x,y)}^2L)$ can be expected to give strong responses to spatial blob responses whose intensity values vary strongly around local minima or local maxima over time.

By combining these two entities into a quasi quadrature measure $\mathcal{Q}_t(\nabla_{(x,y)}^2L)$ over time, we obtain a differential entity that can be expected to give strong responses when then the intensity varies strongly over both image space and over time, while giving no response if there are no intensity variations over space or time. Hence, these three differential operators could be regarded as a primitive spatio-temporal interest operators that can be seen as compatible with existing knowledge about neural processes in early vision (specifically, the LGN).

Temporal derivatives of the determinant of the spatial Hessian. Inspired by the way local extrema of the determinant of the spatial Hessian (91) can be shown to constitute a better interest point detector than local extrema of the spatial Laplacian (90) (Lindeberg [54, 55]), we can compute corresponding first- and second-order derivatives over time of the determinant of the spatial Hessian

$$\partial_t(\det \mathcal{H}_{(x,y)}L) = L_{xxt}L_{yy} + L_{xx}L_{yyt} - 2L_{xy}L_{xyt} \quad (111)$$

$$\partial_{tt}(\det \mathcal{H}_{(x,y)}L) = L_{xxtt}L_{yy} + 2L_{xxt}L_{yyt} + L_{xx}L_{yytt} - 2L_{xyt}^2 - 2L_{xy}L_{xytt} \quad (112)$$

and combine these entities into a quasi quadrature measure over time

$$\mathcal{Q}_t(\det \mathcal{H}_{(x,y)}L) = (\partial_t(\det \mathcal{H}_{(x,y)}L))^2 + C (\partial_{tt}(\det \mathcal{H}_{(x,y)}L))^2 \quad (113)$$

As the determinant of the spatial Hessian can be expected to give strong responses when there are strong intensity variations in two spatial directions, the corresponding spatio-temporal operator $\mathcal{Q}_t(\det \mathcal{H}_{(x,y)}L)$ can be expected to give strong responses at such spatial points at which there are additionally strong intensity variations over time as well.

Genuinely spatio-temporal interest operators. A less temporal slice oriented and more genuine 3-D spatio-temporal approach to defining interest point detectors from second-order spatio-temporal derivatives is by considering feature detectors such as *the determinant of the spatio-temporal Hessian matrix*

$$\det \mathcal{H}_{(x,y,t)}L = L_{xx}L_{yy}L_{tt} + 2L_{xy}L_{xt}L_{yt} - L_{xx}L_{yt}^2 - L_{yy}L_{xt}^2 - L_{tt}L_{xy}^2, \quad (114)$$

the *spatio-temporal Gaussian curvature*

$$\det \mathcal{G}_{(x,y,t)}L = ((L_t(L_{xx}L_t - 2L_xL_{xt}) + L_x^2L_{tt})(L_t(L_{yy}L_t - 2L_yL_{yt}) + L_y^2L_{tt}) - (L_t(-L_xL_{yt} + L_{xy}L_t - L_{xt}L_y) + L_xL_yL_{tt})^2) / L_t^2, \quad (115)$$

or possibly trying to define a *spatio-temporal Laplacian*

$$\nabla_{(x,y,t)}^2L = L_{xx} + L_{yy} + \varkappa^2L_{tt}. \quad (116)$$

Detection of local extrema of the determinant of the spatio-temporal Hessian has been proposed as a spatio-temporal interest point detector by (Willems *et al.* [80]). Properties of the 3-D Gaussian curvature have been studied in (Lindeberg [54]).

If aiming at defining a spatio-temporal analogue of the Laplacian operator, one does, however, need to consider that the most straightforward way of defining such an operator $\nabla_{(x,y,t)}^2L = L_{xx} + L_{yy} + L_{tt}$ is not covariant under independent scaling of the spatial and temporal coordinates as occurs of observing the same scene with cameras having independently different spatial and temporal sampling rates. Therefore, the choice of the relative weighting factor \varkappa^2 between temporal *vs.* spatial derivatives introduced in equation (116) is in principle arbitrary. By the homogeneity of the determinant of the Hessian (114) and the spatio-temporal Gaussian curvature (115) in terms of the orders of spatial *vs.* temporal differentiation that are multiplied in each term, these expressions are on the other hand truly covariant under independent rescalings of the spatial and temporal coordinates and therefore better candidates for being used as spatio-temporal interest operators unless the relative scaling and weighting of temporal *vs.* spatial coordinates can be handled by some complementary mechanism.

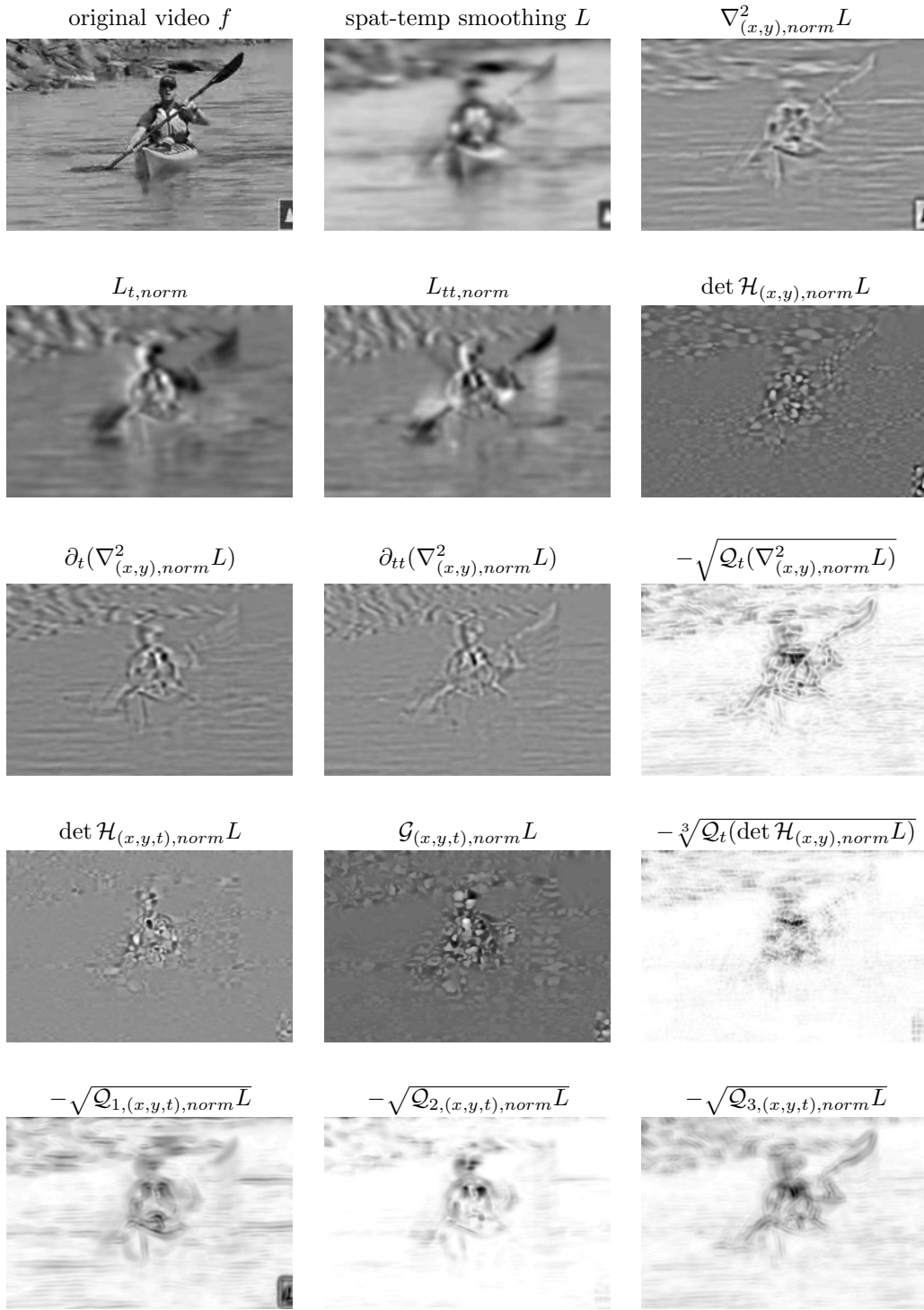


Figure 7: Spatio-temporal feature responses computed from a video sequence in the UCF-101 dataset (Kayaking_g01.c01.avi, cropped) at spatial scale $\sigma_x = 2$ pixels and temporal scale $\sigma_t = 0.2$ seconds using the proposed separable spatio-temporal receptive field model with Gaussian filtering over the spatial domain and here a cascade of 7 recursive filters over the temporal domain with a logarithmic distribution of the intermediate scale levels for $c = \sqrt{2}$ and with L_p -normalization of both the spatial and temporal derivative operators. Each figure shows a snapshot around frames 90-97 for the spatial or spatio-temporal differential expression shown above the figure with in some cases additional monotone stretching of the magnitude values to simplify visual interpretation. (Image size: 258×172 pixels of original 320×240 pixels and 226 frames.)

Spatio-temporal quasi quadrature entities. Inspired by the way the spatial quasi quadrature measure $\mathcal{Q}_{(x,y)}L$ in (96) is defined as a measure of the amount of information in first- and second-order spatial derivatives, we may consider different types of spatio-temporal extensions of this entity

$$\begin{aligned} \mathcal{Q}_{1,(x,y,t)}L &= L_x^2 + L_y^2 + \varkappa^2 L_t^2 + \\ &\quad + C(L_{xx}^2 + 2L_{xy}^2 + L_{yy}^2 + \varkappa^2(L_{xt}^2 + L_{yt}^2) + \varkappa^4 L_{tt}^2) \end{aligned} \quad (117)$$

$$\begin{aligned} \mathcal{Q}_{2,(x,y,t)}L &= \mathcal{Q}_t L \times \mathcal{Q}_{(x,y)}L \\ &= (L_t^2 + C L_{tt}^2)(L_x^2 + L_y^2 + C(L_{xx}^2 + 2L_{xy}^2 + L_{yy}^2)) \end{aligned} \quad (118)$$

$$\begin{aligned} \mathcal{Q}_{3,(x,y,t)}L &= \mathcal{Q}_{(x,y)}L_t + C \mathcal{Q}_{(x,y)}L_{tt} \\ &= L_{xt}^2 + L_{yt}^2 + C(L_{xxt}^2 + 2L_{xyt}^2 + L_{yyt}^2) \\ &\quad + C(L_{xxtt}^2 + L_{yytt}^2 + C(L_{xxtt}^2 + 2L_{xytt}^2 + L_{yytt}^2)) \end{aligned} \quad (119)$$

where in the first expression when needed because of different dimensionalities in terms of spatial *vs.* temporal derivatives, a free parameter \varkappa has been included to adapt the differential expressions to unknown relative scaling and thus weighting between the temporal *vs.* spatial dimensions.

The formulation of these and earlier quasi quadrature entities is inspired by the existence of non-linear receptive fields in the primary visual cortex that do not obey the superposition principle and whose response properties are rather insensitive to the phase of the visual stimuli. Such cells for which the response properties are independent of the polarity of the stimuli are referred to as *complex cells* (Hubel and Wiesel [28, 29]). Specifically, results by De Valois *et al.* [76] show that first- and second-order receptive fields typically occur in pairs that can be modelled as approximate Hilbert pairs. Within the framework of the presented spatio-temporal scale-space concept, it is interesting to note that non-linear receptive fields with qualitatively similar properties can be constructed by squaring first- and second-order derivative responses and summing up these components (Koenderink and van Doorn [37]). The use of quasi quadrature model can therefore be interpreted as a Gaussian-derivative-based analogue of the energy model for complex cells proposed by (Adelson and Bergen [1]; Heeger [27]). To obtain local phase independence over variations over both space and time simultaneously, we do here additionally extend the notion of quasi quadrature to composed space-time, by simultaneously summing up squares of odd and even filter responses over space and time, leading to quadruples or octuples of filter responses, complemented by additional terms to achieve rotational invariance over the spatial domain.

For the first quasi quadrature entity $\mathcal{Q}_{1,(x,y,t)}L$ to respond, it is sufficient if there are intensity variations in the image data either over space or over time. For the second quasi quadrature entity $\mathcal{Q}_{2,(x,y,t)}L$ to respond, it is on the other hand necessary that there are intensity variations in the image data over both space and time. For the third quasi quadrature entity $\mathcal{Q}_{3,(x,y,t)}L$ to respond, it is also necessary that there are intensity variations in the image data over both space and time. Additionally, the third quasi quadrature entity $\mathcal{Q}_{3,(x,y,t)}L$ requires there to be intensity variations over both space and time for each primitive receptive field in terms of plain partial derivatives that is to contribute to the output of the composed quadrature entity. Conceptually, the third quasi quadrature entity can therefore be seen as more related to the form of temporal quasi quadrature entity applied to the idealized model of

LGN cells in (110)

$$\mathcal{Q}_t(\nabla_{(x,y)}^2 L) = \left(\nabla_{(x,y)}^2 L_t\right)^2 + C \left(\nabla_{(x,y)}^2 L_{tt}\right)^2 \quad (120)$$

with the difference that the spatial Laplacian operator $\nabla_{(x,y)}^2$ followed by squaring in (120) is here replaced by the spatial quasi quadrature operator $\mathcal{Q}_{(x,y)}$.

These feature detectors can therefore be seen as biologically inspired change detectors or as ways of measuring the combined strength of a set of receptive fields at any point, as possibly combined with variabilities over other parameters in the family of receptive fields.

Figure 7 shows the result of computing these differential expressions for a video sequence of a paddler in a kayak, using the proposed scale normalization with respect to spatial and temporal scales as described in more detail in next section.

8.5 Scale normalized spatio-temporal derivative expressions

For regular partial derivatives, normalization with respect to spatial and temporal scales of a spatio-temporal scale-space derivative of order $m = (m_1, m_2)$ over space and order n over time is performed according to

$$L_{x_1^{m_1} x_2^{m_2} t^n, norm} = s^{(m_1+m_2)} \alpha_n(\tau) L_{x_1^{m_1} x_2^{m_2} t^n} \quad (121)$$

A similar form of scale normalization applies to spatio-temporal directional derivatives of the form (87) along two spatial orientations φ and $\perp\varphi$ in image space and some motion direction v in space-time

$$L_{\varphi^{m_1} \perp\varphi^{m_2} t^n, norm} = s^{(m_1+m_2)} \alpha_n(\tau) L_{\varphi^{m_1} \perp\varphi^{m_2} t^n} \quad (122)$$

Applied to space-time coupled spatio-temporal derivative expressions as described in previous section, we obtain the following for the scale-normalized temporal derivatives of the Laplacian that can be seen as idealized approximations of space-time separable cells in the LGN

$$\partial_{t, norm}(\nabla_{(x,y), norm}^2 L) = s \alpha_1(\tau) (L_{xxt} + L_{yyt}) = s \alpha_1(\tau) \partial_t(\nabla_{(x,y)}^2 L) \quad (123)$$

$$\partial_{tt, norm}(\nabla_{(x,y), norm}^2 L) = s \alpha_2(\tau) (L_{xxtt} + L_{yytt}) = s \alpha_2(\tau) \partial_{tt}(\nabla_{(x,y)}^2 L) \quad (124)$$

$$\begin{aligned} \mathcal{Q}_{t, norm}(\nabla_{(x,y), norm}^2 L) &= \left(\partial_{t, norm}(\nabla_{(x,y), norm}^2 L)\right)^2 + \left(\partial_{tt, norm}(\nabla_{(x,y), norm}^2 L)\right)^2 \\ &= s^2 (\alpha_1^2(\tau) (L_{xxt} + L_{yyt})^2 + C \alpha_2^2(\tau) (L_{xxtt} + L_{yytt})^2), \end{aligned} \quad (125)$$

for the scale-normalized determinant of the spatio-temporal Hessian

$$\begin{aligned} \det \mathcal{H}_{(x,y,t), norm} L &= s^2 (\alpha_2(\tau) L_{xx} L_{yy} L_{tt} + 2\alpha_1^2(\tau) L_{xy} L_{xt} L_{yt} \\ &\quad - \alpha_1^2(\tau) (L_{xx} L_{yt}^2 - L_{yy} L_{xt}^2) - \alpha_2(\tau) L_{tt} L_{xy}^2), \end{aligned} \quad (126)$$

for the scale-normalized rescaled Gaussian curvature

$$\begin{aligned} \det \mathcal{G}_{(x,y,t), norm} L &= s^2 ((\alpha_1^2(\tau) L_t (L_{xx} L_t - 2L_x L_{xt}) + \alpha_2(\tau) L_x^2 L_{tt}) \times \\ &\quad (\alpha_1^2(\tau) L_t (L_{yy} L_t - 2L_y L_{yt}) + \alpha_2(\tau) L_y^2 L_{tt}) \\ &\quad - (\alpha_1^2(\tau) L_t (-L_x L_{yt} + L_{xy} L_t - L_{xt} L_y) + \alpha_2(\tau) L_x L_y L_{tt})^2) \\ &\quad / (\alpha_1^2(\tau) L_t^2). \end{aligned} \quad (127)$$

and if we attempt to define a scale-normalized spatio-temporal Laplacian

$$\nabla_{(x,y,t),norm}^2 L = s^2(L_{xx} + L_{yy}) + \alpha_2(\tau) \varkappa^2 L_{tt}. \quad (128)$$

For the three different spatio-temporal quadrature entities, the corresponding scale-normalized expressions are in turn given by

$$\begin{aligned} \mathcal{Q}_{1,(x,y,t),norm} L &= s(L_x^2 + L_y^2) + \alpha_1^2(\tau) \varkappa^2 L_t^2 + \\ &\quad + C(s^2(L_{xx}^2 + 2L_{xy}^2 + L_{yy}^2) \\ &\quad + s\alpha_1^2(\tau) \varkappa^2(L_{xt}^2 + L_{yt}^2) + \alpha_2^2(\tau) \varkappa^4 L_{tt}^2) \end{aligned} \quad (129)$$

$$\begin{aligned} \mathcal{Q}_{2,(x,y,t),norm} L &= \mathcal{Q}_{t,norm} L \times \mathcal{Q}_{(x,y),norm} L \\ &= (\alpha_1^2(\tau) L_t^2 + C\alpha_2^2(\tau) L_{tt}^2) \times \\ &\quad (s(L_x^2 + L_y^2) + C s^2(L_{xx}^2 + 2L_{xy}^2 + L_{yy}^2)) \end{aligned} \quad (130)$$

$$\begin{aligned} \mathcal{Q}_{3,(x,y,t),norm} L &= \mathcal{Q}_{(x,y),norm} L_t + C \mathcal{Q}_{(x,y),norm} L_{tt} \\ &= \alpha_1^2(\tau) (s(L_{xt}^2 + L_{yt}^2) + C s^2(L_{xxt}^2 + 2L_{xyt}^2 + L_{yyt}^2)) \\ &\quad + C\alpha_2^2(\tau) (s(L_{xtt}^2 + L_{ytt}^2) + C s^2(L_{xxtt}^2 + 2L_{xytt}^2 + L_{yytt}^2)) \end{aligned} \quad (131)$$

8.6 Geometric covariance and invariance properties

Rotations in image space. A single partial derivative $L_{x_1^{m_1} x_2^{m_1} t^n}(x_1, x_2, t; s, \tau)$ (83) or directional derivative $L_{\varphi^{m_1} \perp \varphi^{m_2} t^n}$ (87) is obviously not rotationally invariant, although the full family of such partial derivatives or directional derivatives may emulate rotational invariance by the steerability of directional derivative operators (85) and (86) which follows directly from the definition of the directional derivative operators ∂_φ , $\partial_{\perp\varphi}$ and ∂_{t_v} . Since the scale normalization factors of such partial derivative or directional derivative operators are all equal within the same order of spatial and temporal differentiation (121) and (122), this steerability property does therefore extend also to scale-normalized partial derivatives or directional derivatives.

The previously mentioned spatial differential expressions $|\nabla_{(x,y)} L|$, $\nabla_{(x,y)}^2 L$, $\det \mathcal{H}_{(x,y)}$, \tilde{L}_{vv} , L_{pp} , L_{qq} , $\tilde{\kappa}(L)$ and $\mathcal{Q}_{(x,y)} L$ are all invariant under rotations in the image domain and so are their corresponding scale-normalized expressions. The previously mentioned spatio-temporal derivative expressions $\partial_t(\nabla_{(x,y)}^2 L)$, $\partial_{tt}(\nabla_{(x,y)}^2 L)$, $\mathcal{Q}_t(\nabla_{(x,y)}^2 L)$, $\partial_t(\det \mathcal{H}_{(x,y)} L)$, $\partial_{tt}(\det \mathcal{H}_{(x,y)} L)$, $\mathcal{Q}_t(\det \mathcal{H}_{(x,y)} L)$, $\det \mathcal{H}_{(x,y,t)} L$, $\det \mathcal{G}_{(x,y,t)} L$, $\nabla_{(x,y,t)}^2 L$, $\mathcal{Q}_{1,(x,y,t)} L$, $\mathcal{Q}_{2,(x,y,t)} L$ and $\mathcal{Q}_{3,(x,y,t)} L$ are also invariant under rotations in the image domain and so are their corresponding scale-normalized expressions.

Uniform rescaling of the spatial domain. Under a uniform scaling transformation of image space, the spatial differential expressions $|\nabla_{(x,y)} L|$, $\nabla_{(x,y)}^2 L$, $\det \mathcal{H}_{(x,y)}$, \tilde{L}_{vv} , L_{pp} , L_{qq} and $\tilde{\kappa}(L)$ are covariant under spatial scaling transformations in the sense that their magnitude values are multiplied by a power of the scaling factor, and so are their corresponding scale-normalized expressions. Also the spatio-temporal derivative expressions $\partial_t(\nabla_{(x,y)}^2 L)$, $\partial_{tt}(\nabla_{(x,y)}^2 L)$, $\partial_t(\det \mathcal{H}_{(x,y)} L)$, $\partial_{tt}(\det \mathcal{H}_{(x,y)} L)$, $\det \mathcal{H}_{(x,y,t)} L$ and $\det \mathcal{G}_{(x,y,t)} L$ and their corresponding scale-normalized expressions are covariant under spatial scaling transformations in the sense that their magnitude values are multiplied by a power of the scaling factor under such spatial scaling transformations.

The quasi quadrature entity $\mathcal{Q}_{(x,y)} L$ is however not covariant under spatial scaling transformations and not the spatio-temporal derivative expressions $\mathcal{Q}_t(\nabla_{(x,y)}^2 L)$,

$\mathcal{Q}_t(\det \mathcal{H}_{(x,y)}L)$, $\mathcal{Q}_{1,(x,y,t)}L$, $\mathcal{Q}_{2,(x,y,t)}L$ and $\mathcal{Q}_{3,(x,y,t)}L$ either. Due to the form of $\mathcal{Q}_{(x,y)}L$, $\mathcal{Q}_t(\nabla_{(x,y)}^2L)$, $\mathcal{Q}_t(\det \mathcal{H}_{(x,y)}L)$, $\mathcal{Q}_{2,(x,y,t)}L$ and $\mathcal{Q}_{3,(x,y,t)}L$ as being composed of sums of scale-normalized derivative expressions for $\gamma = 1$, these derivative expressions can, however, anyway be made scale invariant when combined with a spatial scale selection mechanism.

Uniform rescaling of the temporal domain independent of the spatial domain. Under an independent rescaling of the temporal dimension while keeping the spatial dimension fixed, the partial derivatives $L_{x_1^{m_1}x_2^{m_2}t^n}(x_1, x_2, t; s, \tau)$ are covariant under such temporal rescaling transformations, and so are the directional derivatives $L_{\varphi^{m_1} \perp \varphi^{m_2} t^n}$ for image velocity $v = 0$. For non-zero image velocities, the image velocities would on the other hand need to be adapted to the new temporal axis to enable matching between corresponding spatio-temporal directional derivative operators.

Under an independent rescaling of the temporal dimension while keeping the spatial dimension fixed, also the spatio-temporal derivative expressions $\partial_t(\nabla_{(x,y)}^2L)$, $\partial_{tt}(\nabla_{(x,y)}^2L)$, $\partial_t(\det \mathcal{H}_{(x,y)}L)$, $\partial_{tt}(\det \mathcal{H}_{(x,y)}L)$, $\det \mathcal{H}_{(x,y,t)}L$ and $\det \mathcal{G}_{(x,y,t)}L$ are covariant under independent rescaling of the temporal *vs.* spatial dimensions. The same applies to their corresponding scale-normalized expressions.

The spatio-temporal derivative expressions $\mathcal{Q}_t(\nabla_{(x,y)}^2L)$, $\mathcal{Q}_t(\det \mathcal{H}_{(x,y)}L)$, $\mathcal{Q}_{1,(x,y,t)}L$, $\mathcal{Q}_{2,(x,y,t)}L$ and $\mathcal{Q}_{3,(x,y,t)}L$ are however not covariant under independent rescaling of the temporal *vs.* spatial dimensions and would therefore need a temporal scale selection mechanism to enable temporal scale invariance.

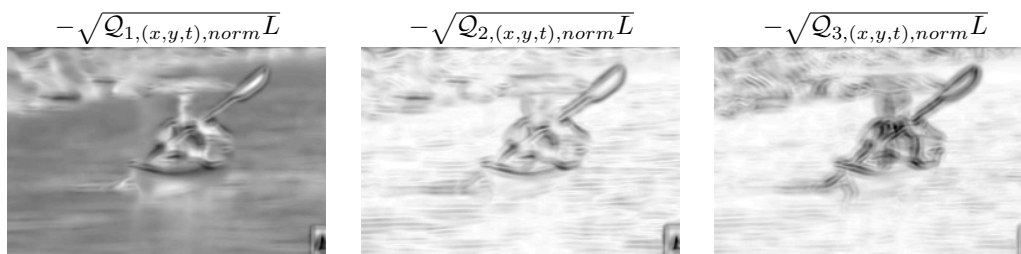


Figure 8: Illustration of the influence of temporal illumination or exposure compensation mechanisms on spatio-temporal receptive field responses, computed from the video sequence Kayaking_g01_c01.avi (cropped) in the UCF-101 dataset. Each figure shows a snapshot at frame 8 for the quasi quadrature entity shown above the figure with additional monotone stretching of the magnitude values to simplify visual interpretation. Notice how the time varying illumination or exposure compensation leads to a strong overall response in the first quasi quadrature entity $\mathcal{Q}_{1,(x,y,t),norm}L$ caused by strong responses in the purely temporal derivatives L_t and L_{tt} , whereas the responses of second and the third quasi quadrature entities $\mathcal{Q}_{2,(x,y,t),norm}L$ and $\mathcal{Q}_{3,(x,y,t),norm}L$ are much less influenced. Indeed, for a logarithmic brightness scale the third quasi quadrature entity $\mathcal{Q}_{3,(x,y,t),norm}L$ is invariant under such multiplicative illumination or exposure compensations variations.

8.7 Invariance to illumination variations and exposure control mechanisms

Because of all these expressions being composed of spatial, temporal and spatio-temporal derivatives of non-zero order, it follows that all these differential expressions are invariant under additive illumination transformations of the form $L \mapsto L + C$.

This means that if we would take the image values f as representing the logarithm of the incoming energy $f \sim \log I$ or $f \sim \log I^\gamma = \gamma \log I$, then all these differential expressions will be invariant under local multiplicative illumination transformations of the form $I \mapsto CI$ implying $L \sim \log I + \log C$ or $L \sim \log I^\gamma = \gamma(\log I + \log C)$. Thus, these differential expressions will be invariant to local multiplicative variabilities in the external illumination (with locality defined as the support region of the spatio-temporal receptive field) or multiplicative exposure control parameters such as the aperture of the lens and integration time or the sensitivity of the sensor.

More formally, let us assume a (i) perspective camera model extended with (ii) a thin circular lens for gathering incoming light from different directions and (iii) a Lambertian illumination model extended with (iv) a spatially varying albedo factor for modelling the light that is reflects from surface patterns in the world. Then, it can be shown (Lindeberg [52, section 2.3]) that a spatial receptive field response

$$L_{x^{m_1}y^{m_2}t^n}(\cdot, \cdot; s, \tau) = \partial_{x^{m_1}y^{m_2}t^n} (T(\cdot, \cdot; s, \tau) * f(\cdot, \cdot)) \quad (132)$$

of the image data f , where $T(\cdot, \cdot; s, \tau)$ represents the spatio-temporal smoothing operator can be expressed as

$$L_{x^{m_1}y^{m_2}t^n} = \partial_{x^{m_1}y^{m_2}t^n} \mathcal{T}_s \left(\log \rho(x, y, t) + \log i(x, y, t) + \log C_{cam}(\tilde{f}(t)) + V(x, y) \right) \quad (133)$$

where

- (i) $\rho(x, y, t)$ is a spatially dependent *albedo factor* that reflects *properties of surfaces of objects* in the environment with the implicit understanding that this entity may in general refer to points on different surfaces in the world depending on the viewing direction and thus the image position (x, y) and depending on time t because of relative motions between objects in the world and the observer,
- (ii) $i(x, y, t)$ denotes a spatially dependent *illumination field* with the implicit understanding that the amount of incoming light on different surfaces may be different for different points in the world as mapped to corresponding image coordinates (x, y) and may vary over time t ,
- (iii) $C_{cam}(\tilde{f}(t)) = \frac{\pi d}{4 \tilde{f}}$ represents possibly time-varying *internal camera parameters* with the ratio $\tilde{f} = f/d$ referred to as the *effective f-number*, where d denotes the diameter of the lens and f the focal distance and
- (iv) $V(x, y) = -2 \log(1 + x^2 + y^2)$ represents a geometric *natural vignetting* effect corresponding to the factor $\log \cos^4(\phi)$ for a planar image plane, with ϕ denoting the angle between the viewing direction (x, y, f) and the surface normal $(0, 0, 1)$ of the image plane. This vignetting term disappears for a spherical camera model.

From the structure of equation (133) we can note that for any non-zero order of spatial differentiation $m_1 + m_2 > 0$, the influence of the internal camera parameters in $C_{cam}(\tilde{f}(t))$ will disappear because of the spatial differentiation with respect to x_1 or x_2 , and so will the effects of any other multiplicative exposure control mechanism. Furthermore, for any multiplicative illumination variation $i'(x, y) = Ci(x, y)$, where C is a scalar constant, the logarithmic luminosity will be transformed as $\log i'(x, y) = \log C + \log i(x, y)$, which implies that the dependency on C will disappear after spatial

differentiation. For purely temporal derivative operators, that do not involve any order of spatial differentiation, such as the first- and second-order derivative operators, L_t and L_{tt} , strong responses may on the other hand be obtained due to illumination compensation mechanisms that vary over time as the results of rapid variations in the illumination. If one wants to design spatio-temporal feature detectors that are robust to illumination variations and to variations in exposure compensation mechanisms caused by these, it is therefore essential to include non-zero orders of spatial variation. The use of Laplacian-like filtering in the first stages of visual processing in the retina and the LGN can therefore be interpreted as an aptly design to achieve robustness of illumination variations and adaptive variations in the diameter of the pupil caused by these, while still being expressed in terms of rotationally symmetric receptive fields over the spatial domain.

If we extend this model to the simplest form of position- and time-dependent illumination and/or exposure variation model of the form

$$L \mapsto L + Ax + By + Ct \tag{134}$$

then we can see that the spatio-temporal derivative expressions $\partial_t(\nabla_{(x,y)}^2 L)$, $\partial_{tt}(\nabla_{(x,y)}^2 L)$, $\mathcal{Q}_t(\nabla_{(x,y)}^2 L)$, $\partial_t(\det \mathcal{H}_{(x,y)} L)$, $\partial_{tt}(\det \mathcal{H}_{(x,y)} L)$, $\mathcal{Q}_t(\det \mathcal{H}_{(x,y)} L)$, $\det \mathcal{H}_{(x,y,t)} L$, $\det \mathcal{G}_{(x,y,t)} L$, $\nabla_{(x,y,t)}^2 L$ and $\mathcal{Q}_{3,(x,y,t)} L$ are all invariant under such position- and time-dependent illumination and/or exposure variations.

The quasi quadrature entities $\mathcal{Q}_{1,(x,y,t)} L$ and $\mathcal{Q}_{2,(x,y,t)} L$ are however not invariant to such position- and time-dependent illumination variations. This property can in particular be noted for the quasi quadrature entity $\mathcal{Q}_{1,(x,y,t)} L$ where for which seems as initial time-varying exposure compensation mechanisms in the camera lead to large responses in the initial part of the video sequence (see figure 8(left)). Out of the three quasi quadrature entities $\mathcal{Q}_{1,(x,y,t)} L$, $\mathcal{Q}_{2,(x,y,t)} L$ and $\mathcal{Q}_{3,(x,y,t)} L$, the third quasi quadrature entity does therefore possess the best robustness properties to illumination variations (see figure 8(right)).

9 Summary and discussion

We have presented an improved computational model for spatio-temporal receptive fields based on time-causal and time-recursive spatio-temporal scale-space representation defined from a set of first-order integrators or truncated exponential filters coupled in cascade over the temporal domain in combination with a Gaussian scale-space concept over the spatial domain. This model can be efficiently implemented in terms of recursive filters and we have shown how the continuous model can be transferred to a discrete implementation while retaining discrete scale-space properties. Specifically, we have analysed how remaining design parameters within the theory, in terms of the number of first-order integrators coupled in cascade and a distribution parameter of a logarithmic distribution, affect the temporal response dynamics in terms of temporal delays.

Compared to other spatial and temporal scale-space representations based on continuous scale parameters, a conceptual difference with the temporal scale-space representation underlying the proposed spatio-temporal receptive fields, is that the temporal scale levels have to be discrete. Thereby, we sacrifice full scale invariance as resulting from Gaussian scale-space concepts based on causality or non-enhancement of local extrema (Koenderink [35]; Lindeberg [51]) or used as a scale-space axiom in certain axiomatic scale-space formulations (Iijima [31]; Florack et al. [20]; Pauwels

et al. [63]; Weickert et al. [78, 77, 79]; Duits et al. [11, 12]; Fagerström [13, 14]); see also Witkin [81], Babaud *et al.* [3], Yuille and Poggio [82], Koenderink and van Doorn [37, 38], Lindeberg [40, 43, 44, 45, 46, 53], Florack et al. [19, 20, 18], Alvarez *et al.* [2], Guichard [24], ter Haar Romeny *et al.* [26, 25], Felsberg and Sommer [16] and Tschirsich and Kuijper [74] for other scale-space approaches closely related to this work, as well as Fleet and Langley [17], Freeman and Adelson [23], Simoncelli *et al.* [73] and Perona [64] for more filter-oriented approaches, Miao and Rao [61], Duits and Burgeth [10], Cocci *et al.* [7], Barbieri *et al.* [4] and Sharma and Duits [75] for Lie group approaches for receptive fields and Lindeberg and Friberg [59] for the application of closely related principles for deriving idealized computational models of auditory receptive fields.

When using a logarithmic distribution of the intermediate scale levels, we have however shown that by a limit construction when the number of intermediate temporal scale levels tends to infinity, we can achieve true self-similarity and scale invariance over a discrete set of scaling factors. For a vision system intended to operate in real time using no other explicit storage of visual data from the past than a compact time-recursive buffer of spatio-temporal scale-space at different temporal scales, the loss of a continuous temporal scale parameter may however be less of a practical constraint, since one would anyway have to discretize the temporal scale levels in advance to be able to register the image data to be able to perform any computations at all.

In the special case when all the time constants of the first-order integrators are equal, the resulting temporal smoothing kernels in the continuous model (29) correspond to Laguerre functions, which have been previously used for modelling the temporal response properties of neurons in the visual system (den Brinker and Roufs [6]) and for computing spatio-temporal image features in computer vision (Rivero-Moreno and Bres [65]; Berg et al. [5]). Regarding the corresponding discrete model with all time constants equal, the corresponding discrete temporal smoothing kernels approach Poisson kernels when the number of temporal smoothing steps increases while keeping the variance of the composed kernel fixed (Lindeberg and Fagerström [58]). Such Poisson kernels have also been used for modelling biological vision (Fourtes and Hodgkin [22]). Compared to the special case with all time constants equal, a logarithmic distribution of the intermediate temporal scale levels (16) does on the other hand allow for larger flexibility in the trade-off between temporal smoothing and temporal response characteristics, specifically enabling faster temporal responses (shorter temporal delays) and higher computational efficiency when computing multiple temporal or spatio-temporal receptive field responses involving coarser temporal scales.

From the detailed analysis in section 5 and appendix A we can conclude that when the number of first-order integrators that are coupled in cascade increases while keeping the variance of the composed kernel fixed, the time-causal kernels obtained by composing truncated exponential kernels with equal time constants in cascade tend to a limit kernel with skewness and kurtosis measures zero, or equivalently third- and fourth-order cumulants equal to zero, whereas the time-causal kernels obtained by composing truncated exponential kernels having a logarithmic distribution of the intermediate scale levels tends to a limit kernel with non-zero skewness and non-zero kurtosis. This property reveals a fundamental difference between the two classes of time-causal scale-space kernels based on either a logarithmic or a uniform distribution of the intermediate temporal scale levels.

In a complementary analysis in appendix B, we have also shown how our time-causal kernels can be related to the temporal kernels in Koenderink's scale-time model

[36]. By identifying the first- and second-order temporal moments of the two classes of kernels, we have derived closed-form expressions to relate the parameters between the two models, and showed that although the two classes of kernels to a large extent share qualitatively similar properties, the two classes of kernels differ significantly in terms of their third- and fourth-order skewness and kurtosis measures.

The closed-form expressions for Koenderink’s scale-time kernels are analytically simpler than the explicit expressions for our kernels, which will be sums of truncated exponential kernels for all the time constants with the coefficients determined from a partial fraction expansion. In this respect, the derived mapping between the parameters of our and Koenderink’s models can be used *e.g.* for estimation the time of the temporal maximum of our kernels, which would otherwise have to be determined numerically. Our kernels do on the other hand have a clear computational advantage in that they are truly time-recursive, meaning that the primitive first-order integrators in the model contain sufficient information for updating the model to new states over time, whereas the kernels in Koenderink’s scale-time model appear to require a complete memory of the past, since they do not have any known time-recursive formulation.

Given the derived time-causal and time-recursive formulation of our primitive spatio-temporal receptive fields, we have described how this theory can be used for computing different types of scale-normalized spatio-temporal features. Specifically, we have emphasized how scale normalization by L_p -normalization leads to fundamentally different results compared to a more traditional approach of variance-based normalization. By the formulation of the corresponding scale normalization factors for discrete temporal scale space, we have also shown how they permit the formulation of an operational criterion to estimate how many intermediate temporal scale levels are needed to approximate true scale invariance up to a given tolerance.

Finally, we have shown how different types of spatio-temporal features can be defined in terms of spatio-temporal differential invariants built from spatio-temporal receptive field responses, including their transformation properties under natural image transformations, with emphasis on independent scaling transformations over space *vs.* time, rotational invariance over the spatial domain and illumination and exposure control variations. We propose that the presented theory can be used for building features for generic purposes in computer vision and for computational modelling of biological vision for image data over a time-causal spatio-temporal domain, in an analogous way as the Gaussian scale-space concept constitutes a canonical model for processing image data over a purely spatial domain.

Acknowledgements

An earlier version of this work has been accepted for the SSVM 2015 conference [56].

A Frequency analysis of the time-causal kernels

In this appendix, we will perform an in-depth analysis of the proposed time-causal scale-space kernels with regard to their frequency properties and moment descriptors derived via the Fourier transform, both for the case of a logarithmic distribution of the intermediate temporal scale levels and a uniform distribution of the intermediate temporal scale levels. Specifically, the results to be derived will provide a way to characterize properties of the limit kernel when the number of temporal scale levels

K tends to infinity.

A.1 Logarithmic distribution of the intermediate scale levels

In section 5, we gave the following explicit expressions for the Fourier transform of the time-causal kernels based on a logarithmic distribution of the intermediate scale levels

$$\hat{h}_{exp}(\omega; \tau, c, K) = \frac{1}{1 + i c^{1-K} \sqrt{\tau} \omega} \prod_{k=2}^K \frac{1}{1 + i c^{k-K-1} \sqrt{c^2 - 1} \sqrt{\tau} \omega} \quad (135)$$

for which the magnitude and the phase are given by

$$|\hat{h}_{exp}(\omega; \tau, c, K)| = \frac{1}{\sqrt{1 + c^{2(1-K)} \tau \omega^2}} \prod_{k=2}^K \frac{1}{\sqrt{1 + c^{2(k-K-1)} (c^2 - 1) \tau \omega^2}} \quad (136)$$

$$\arg \hat{h}_{exp}(\omega; \tau, c, K) = \arctan(c^{1-K} \sqrt{\tau} \omega) + \sum_{k=2}^K \arctan(c^{k-K-1} \sqrt{c^2 - 1} \sqrt{\tau} \omega) \quad (137)$$

Let us rewrite the magnitude of the Fourier transform on exponential form

$$\begin{aligned} |\hat{h}_{exp}(\omega; \tau, c, K)| &= e^{\log |\hat{h}_{exp}(\omega; \tau, c, K)|} \\ &= e^{-\frac{1}{2} \log(1 + c^{2(1-K)} \tau \omega^2) - \frac{1}{2} \sum_{k=2}^K \log(1 + c^{2(k-K-1)} (c^2 - 1) \tau \omega^2)} \end{aligned} \quad (138)$$

and compute the Taylor expansion of

$$\log |\hat{h}_{exp}(\omega; \tau, c, K)| = C_2 \omega^2 + C_4 \omega^4 + \mathcal{O}(\omega^6) \quad (139)$$

where

$$C_2 = -\frac{\tau}{2} \quad (140)$$

$$C_4 = -\frac{\tau^2 (-2c^{4-4K} - c^2 + 1)}{4(c^2 + 1)} \rightarrow \frac{(c^2 - 1) \tau^2}{4(c^2 + 1)} \quad (141)$$

and the rightmost expression for C_4 shows the limit value when the number K of first-order integrators coupled in cascade tends to infinity.

Let us next compute the Taylor expansion of

$$\arg \hat{h}_{exp}(\omega; \tau, c, K) = C_1 \omega + C_3 \omega^3 + \mathcal{O}(\omega^5) \quad (142)$$

where the coefficients are given by

$$C_1 = \frac{\sqrt{\tau} c^{-K} (-c^2 + \sqrt{c^2 - 1} c - \sqrt{c^2 - 1} c^K + c)}{c - 1} \rightarrow -\frac{\sqrt{(c^2 - 1)} \sqrt{\tau}}{c - 1} \quad (143)$$

$$\begin{aligned} C_3 &= \frac{\sqrt{c^2 - 1} \tau^{3/2} (c^{3K} + c^{3K+1} - c^4 - c^3) c^{-3K} + (c^5 + c^4 + c^3) \tau^{3/2} c^{-3K}}{3(c^2 + c + 1)} \\ &\rightarrow \frac{(c + 1) \sqrt{c^2 - 1} \tau^{3/2}}{3(c^2 + c + 1)} \end{aligned} \quad (144)$$

and again the rightmost expressions for C_1 and C_3 show the limit values when the number K of scale levels tends to infinity.

Following the definition of cumulants κ_n defined as the Taylor coefficients of the logarithm of the Fourier transform

$$\log h(\omega) = \sum_{n=0}^{\infty} \kappa_n \frac{(-i\omega)^n}{n!} \quad (145)$$

we obtain

$$\begin{aligned} \log \hat{h}_{exp}(\omega; \tau, c, K) &= -C_1(-i\omega) - C_2(-i\omega)^2 + C_3(-i\omega)^3 + C_4(-i\omega)^4 + \mathcal{O}(i\omega^5) \\ &= \kappa_0 + \frac{\kappa_1}{1!}(-i\omega) + \frac{\kappa_2}{2!}(-i\omega^2) + \frac{\kappa_3}{3!}(-i\omega)^3 + \frac{\kappa_4}{4!}(-i\omega)^4 + \mathcal{O}(i\omega^5) \end{aligned} \quad (146)$$

and can read the cumulants of the underlying temporal scale-space kernel as $\kappa_0 = 0$, $\kappa_1 = -C_1$, $\kappa_2 = -2C_2$, $\kappa_3 = 6C_3$ and $\kappa_4 = 24C_4$. Specifically, the first-order moment M_1 and the higher-order central moments M_2 , M_3 and M_4 are related to the cumulants according to

$$M_1 = \kappa_1 = -C_1 \rightarrow \frac{\sqrt{(c^2 - 1)} \sqrt{\tau}}{c - 1} \quad (147)$$

$$M_2 = \kappa_2 = -2C_2 = \tau \quad (148)$$

$$M_3 = \kappa_3 = 6C_3 \rightarrow \frac{2(c+1)\sqrt{c^2-1}\tau^{3/2}}{(c^2+c+1)} \quad (149)$$

$$M_4 = \kappa_4 + 3\kappa_2^2 = 24C_4 + 12C_2^2 \rightarrow \frac{3(3c^2-1)\tau^2}{c^2+1} \quad (150)$$

Thus, the skewness γ_1 and the kurtosis γ_2 measures of the corresponding temporal scale-space kernels are given by

$$\gamma_1 = \frac{\kappa_3}{\kappa_2^{3/2}} = \frac{M_3}{M_2^{3/2}} = \frac{3C_3}{\sqrt{2}(-C_2)^{3/2}} \rightarrow \frac{2(c+1)\sqrt{c^2-1}}{(c^2+c+1)} \quad (151)$$

$$\gamma_2 = \frac{\kappa_4}{\kappa_2^2} = \frac{M_4}{M_2^2} - 3 = 6 \frac{C_4}{C_2^2} \rightarrow \frac{6(c^2-1)}{c^2+1} \quad (152)$$

Figure 9 shows graphs of the limit values of these skewness and kurtosis measures as function of the distribution parameter c for the limit case when the number of scale levels K tends to infinity. As can be seen, both the skewness and the kurtosis measures of the temporal scale-space kernels increase with increasing values of the distribution parameter c .

A.2 Uniform distribution of the intermediate scale levels

When using a uniform distribution of the intermediate scale levels (19), the time constants of the individual first-order integrators are given by (20) and the explicit expression for the Fourier transform (11) is of the form

$$\hat{h}_{exp}(\omega; \tau, K) = \frac{1}{(1 + i \sqrt{\frac{\tau}{K}} \omega)^K} \quad (153)$$

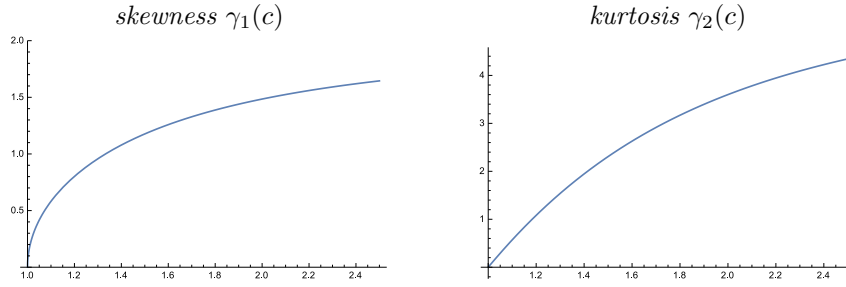


Figure 9: Graphs of the skewness measure γ_1 (151) and the kurtosis measure γ_2 (152) as function of the distribution parameter c for the time-causal scale-space kernels corresponding to limit case of K truncated exponential kernels having a logarithmic distribution of the intermediate scale levels coupled in cascade in the limit case when the number of scale levels K tends to infinity.

Specifically, the magnitude and the phase of the Fourier transform are given by

$$|\hat{h}_{exp}(\omega; \tau, K)| = \frac{1}{\left(1 + \frac{\tau}{K} \omega^2\right)^{K/2}} \quad (154)$$

$$\arg \hat{h}_{exp}(\omega; \tau, K) = -K \arctan \left(\sqrt{\frac{\tau}{K}} \omega \right) \quad (155)$$

Let us rewrite the magnitude of the Fourier transform on exponential form

$$|\hat{h}_{exp}(\omega; \tau, K)| = e^{\log |\hat{h}_{exp}(\omega; \tau, K)|} = e^{-\frac{K}{2} \log(1 + \frac{\tau}{K} \omega^2)} \quad (156)$$

and compute the Taylor expansion of

$$\log |\hat{h}_{exp}(\omega; \tau, K)| = C_2 \omega^2 + C_4 \omega^4 + \mathcal{O}(\omega^6) \quad (157)$$

where

$$C_2 = -\frac{\tau}{2} \quad (158)$$

$$C_4 = \frac{\tau^2}{4K} \quad (159)$$

Next, let us compute the Taylor expansion of

$$\arg \hat{h}_{exp}(\omega; \tau, K) = C_1 \omega + C_3 \omega^3 + \mathcal{O}(\omega^5) \quad (160)$$

where the coefficients are given by

$$C_1 = -\sqrt{K\tau} \quad (161)$$

$$C_3 = \frac{\tau^{3/2}}{3\sqrt{K}} \quad (162)$$

Following the definition of cumulants κ_n according to (145), we can in an analogous to (146) in previous section read $\kappa_0 = 0$, $\kappa_1 = -C_1$, $\kappa_2 = -2C_2$, $\kappa_3 = 6C_3$ and $\kappa_4 =$

$24C_4$, and relate the first-order moment M_1 and the higher-order central moments M_2 , M_3 and M_4 to the cumulants according to

$$M_1 = \kappa_1 = -C_1 = \sqrt{K\tau} \quad (163)$$

$$M_2 = \kappa_2 = -2C_2 = \tau \quad (164)$$

$$M_3 = \kappa_3 = 6C_3 = \frac{2\tau^{3/2}}{\sqrt{K}} \quad (165)$$

$$M_4 = \kappa_4 + 3\kappa_2^2 = 24C_4 + 12C_2^2 = 3\tau^2 + \frac{6\tau^2}{K} \quad (166)$$

Thus, the skewness γ_1 and the kurtosis γ_2 of the corresponding temporal scale-space kernels are given by

$$\gamma_1 = \frac{\kappa_3}{\kappa_2^{3/2}} = \frac{M_3}{M_2^{3/2}} = \frac{2}{\sqrt{K}} \quad (167)$$

$$\gamma_2 = \frac{\kappa_4}{\kappa_2^2} = \frac{M_4}{M_2^2} - 3 = \frac{6}{K} \quad (168)$$

From these expressions we can note that when the number K of first-order integrators that are coupled in cascade increases, these skewness and kurtosis measures tend to zero for the temporal scale-space kernels having a uniform distribution of the intermediate temporal scale levels. The corresponding skewness and kurtosis measures (151) and (152) for the kernels having a logarithmic distribution of the intermediate temporal scale levels do on the other hand remain strictly positive. These properties reveal a fundamental difference between the two classes of time-causal kernels obtained by distributing the intermediate scale levels of first-order integrators coupled in cascade according to a logarithmic *vs.* a uniform distribution.

B Comparison with Koenderink's scale-time model

In his scale-time model, Koenderink [36] proposed to perform a logarithmic mapping of the past via a time delay δ and then applying Gaussian smoothing on the transformed domain, leading to a time-causal kernel of the form, here largely following the notation in Florack [18, result 4.6, page 116]

$$h_{log}(t; \sigma, \delta, a) = \frac{1}{\sqrt{2\pi}\sigma(\delta - a)} e^{-\frac{\log^2\left(\frac{t-a}{\delta-a}\right)}{2\sigma^2}} \quad (169)$$

with a denoting the present moment, δ denoting the time delay and σ is a dimensionless temporal scale parameter relative to the logarithmic time axis. For simplicity, we will henceforth assume $a = 0$ leading to kernels of the form

$$h_{log}(t; \sigma, \delta) = \frac{1}{\sqrt{2\pi}\sigma\delta} e^{-\frac{\log^2\left(\frac{t}{\delta}\right)}{2\sigma^2}} \quad (170)$$

and with convolution reversal of the time axis such that causality implies $h_{log}(t; \sigma, \delta) = 0$ for $t < 0$. By integrating this kernel symbolically in Mathematica, we find

$$\int_{t=-\infty}^{\infty} h_{log}(t; \sigma, \delta) dt = e^{\frac{\sigma^2}{2}} \quad (171)$$

implying that the corresponding time-causal kernel normalized to unit L_1 -norm should be

$$h_{Koe}(t; \sigma, \delta) = \frac{1}{\sqrt{2\pi}\sigma\delta} e^{-\frac{\log^2\left(\frac{t}{\delta}\right) - \frac{\sigma^2}{2}}{2\sigma^2}} \quad (172)$$

The temporal mean of this kernel is

$$M_1 = \bar{t} = \int_{t=-\infty}^{\infty} t h_{Koe}(t; \sigma, \delta) dt = \delta e^{\frac{3\sigma^2}{2}} \quad (173)$$

and the higher-order central moments

$$M_2 = \int_{t=-\infty}^{\infty} (t - \bar{t})^2 h_{Koe}(t; \sigma, \delta) dt = \delta^2 e^{3\sigma^2} (e^{\sigma^2} - 1) \quad (174)$$

$$M_3 = \int_{t=-\infty}^{\infty} (t - \bar{t})^3 h_{Koe}(t; \sigma, \delta) dt = \delta^3 e^{\frac{9\sigma^2}{2}} (e^{\sigma^2} - 1)^2 (e^{\sigma^2} + 2) \quad (175)$$

$$M_4 = \int_{t=-\infty}^{\infty} (t - \bar{t})^4 h_{Koe}(t; \sigma, \delta) dt = \delta^4 e^{6\sigma^2} (e^{\sigma^2} - 1)^2 (3e^{2\sigma^2} + 2e^{3\sigma^2} + e^{4\sigma^2} - 3) \quad (176)$$

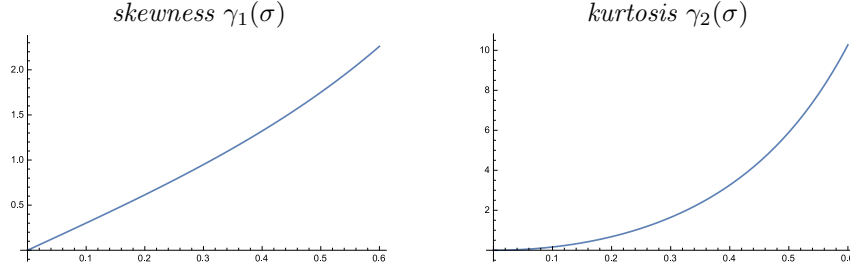


Figure 10: Graphs of the skewness measure γ_1 (177) and the kurtosis measure γ_2 (178) as function of the dimensionless temporal scale parameter σ relative to the logarithmic transformation of the past for the time-causal kernels in Koenderink's scale-time model.

Thus, the skewness γ_1 and the kurtosis γ_2 of the temporal kernels in Koenderink's scale-time model are given by (see figure 10 for graphs)

$$\gamma_1 = \frac{M_3}{M_2^{3/2}} = \sqrt{e^{\sigma^2} - 1} (e^{\sigma^2} + 2) \quad (177)$$

$$\gamma_2 = \frac{M_4}{M_2^2} - 3 = 3e^{2\sigma^2} + 2e^{3\sigma^2} + e^{4\sigma^2} - 6 \quad (178)$$

If we want to relate these kernels in Koenderink's scale-time model to our time-causal scale-space kernels, a natural starting point is to require that the total amount of temporal smoothing as measured by the variances M_2 of the two kernels should be equal. Then, this implies the relation

$$\tau = \delta^2 e^{3\sigma^2} (e^{\sigma^2} - 1) \quad (179)$$

If we additionally relate the kernels by enforcing the temporal delays as measured by the first-order temporal moments to be equal, then we obtain for the limit case when $K \rightarrow \infty$

$$\bar{t} = \sqrt{\frac{c+1}{c-1}} \sqrt{\tau} = \delta e^{\frac{3\sigma^2}{2}} \quad (180)$$

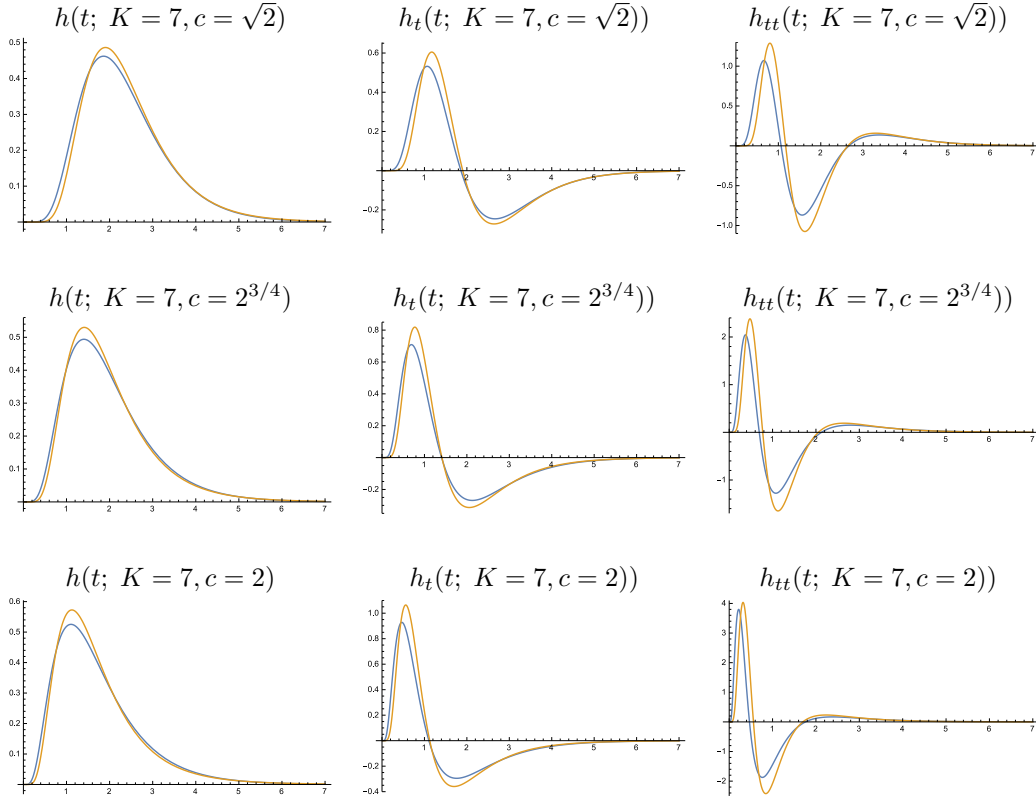


Figure 11: Comparison between the proposed time-causal kernels corresponding to the composition of truncated exponential kernels and in cascade (blue curves) for a logarithmic distribution of the intermediate scale levels and the temporal kernels in Koenderink's scale-time model (brown curves) shown for both the original smoothing kernels and their first- and second-order temporal derivatives. All kernels correspond to temporal scale (variance) $\tau = 1$ with the additional parameters determined such that the temporal mean values (the first-order temporal moments) become equal in the limit case when the number of temporal scale levels K tends to infinity (equation (181)). (top row) Logarithmic distribution of the temporal scale levels for $c = \sqrt{2}$ and $K = 10$. (middle row) Corresponding results for $c = 2^{3/4}$ and $K = 10$. (bottom row) Corresponding results for $c = 2$ and $K = 10$.

Solving the system of equations (179) and (180) then gives the following mappings between the parameters in the two temporal scale-space models

$$\begin{cases} \tau = \delta^2 e^{3\sigma^2} (e^{\sigma^2} - 1) \\ c = \frac{e^{\sigma^2}}{2 - e^{\sigma^2}} \end{cases} \quad \begin{cases} \sigma = \sqrt{\log\left(\frac{2c}{c+1}\right)} \\ \delta = \frac{(c+1)^2 \sqrt{\tau}}{2\sqrt{2}\sqrt{(c-1)c^3}} \end{cases} \quad (181)$$

which hold as long as $c > 1$ and $\sigma < \sqrt{\log 2} \approx 0.832$. Specifically, for small values of σ a series expansion of the relations to the left gives

$$\begin{cases} \tau = \delta^2 \sigma^2 \left(1 + \frac{7\sigma^2}{2} + \frac{37\sigma^4}{6} + \frac{175\sigma^6}{24} + \mathcal{O}(\sigma^8)\right) \\ c = 1 + 2\sigma^2 + 3\sigma^4 + \frac{13\sigma^6}{3} + \mathcal{O}(\sigma^8) \end{cases} \quad (182)$$

If we additionally reparameterize the distribution parameter c such that $c = 2^a$ for some $a > 0$ and perform a series expansion, we obtain

$$a = \frac{\sigma^2 - \log(2 - e^{\sigma^2})}{\log(2)} = \frac{2\sigma^2}{\log 2} \left(1 + \frac{\sigma^2}{2} + \frac{\sigma^4}{2} + \frac{13\sigma^6}{24} + \mathcal{O}(\sigma^8)\right) \quad (183)$$

and with $b = a \log 2$ to simplify the following expressions

$$\begin{cases} \sigma = \frac{\sqrt{b}}{\sqrt{2}} \left(1 - \frac{b}{8} - \frac{b^2}{128} + \frac{13b^3}{3072} + \frac{49b^4}{98304} + \mathcal{O}(b^5)\right) \\ \delta = \frac{\sqrt{2}\sqrt{\tau}}{\sqrt{b}} \left(1 - \frac{3b}{4} + \frac{49b^2}{96} - \frac{31b^3}{128} + \frac{959b^4}{10240} + \mathcal{O}(b^5)\right) \end{cases} \quad (184)$$

These expressions relate the parameters in the two temporal scale-space models in the limit case when the number of temporal scale levels tends to infinity for the time-causal model based on first-order integrators coupled in cascade and with a logarithmic distribution of the intermediate temporal scale levels.

For a general finite value of K , the corresponding relation to (180) that identifies the first-order temporal moments does instead read

$$\bar{t} = \frac{c^{-K} \left(c^2 - \left(\sqrt{c^2 - 1} + 1 \right) c + \sqrt{c^2 - 1} c^K \right)}{c - 1} \sqrt{\tau} = \delta e^{\frac{3\sigma^2}{2}} \quad (185)$$

Solving the system of equations (179) and (185) then gives

$$\begin{cases} \sigma = \sqrt{\log\left(\frac{A}{B}\right)} \\ \delta = \frac{C\sqrt{\tau}}{2\sqrt{2}(c-1)c^K\left(\frac{D}{E}\right)^{3/2}} \end{cases} \quad (186)$$

where

$$\begin{aligned}
A = 2c & \left(c^{4K} - 4c^{K+2} - 4c^{K+3} + 3c^{2K+3} - 3c^{3K+2} + c^{4K+1} + 2c^3 \right. \\
& + \left(\sqrt{c^2 - 1} - 1 \right) c^{3K} - \left(\sqrt{c^2 - 1} - 4 \right) c^{2K+1} \\
& \left. + \left(\sqrt{c^2 - 1} + 5 \right) c^{2K+2} - \left(\sqrt{c^2 - 1} + 4 \right) c^{3K+1} \right) \quad (187)
\end{aligned}$$

$$B = (c^{2K} - 2c^{K+1} - 2c^{K+2} + c^{2K+1} + 2c^2)^2 \quad (188)$$

$$C = \left(c^2 - \left(\sqrt{c^2 - 1} + 1 \right) c + \sqrt{c^2 - 1} c^K \right) \quad (189)$$

$$\begin{aligned}
D = c & \left(c^{4K} - 4c^{K+2} - 4c^{K+3} + 3c^{2K+3} - 3c^{3K+2} + c^{4K+1} + 2c^3 \right. \\
& + \left(\sqrt{c^2 - 1} - 1 \right) c^{3K} - \left(\sqrt{c^2 - 1} - 4 \right) c^{2K+1} \\
& \left. + \left(\sqrt{c^2 - 1} + 5 \right) c^{2K+2} - \left(\sqrt{c^2 - 1} + 4 \right) c^{3K+1} \right) \quad (190)
\end{aligned}$$

$$E = (c^{2K} - 2c^{K+1} - 2c^{K+2} + c^{2K+1} + 2c^2)^2 \quad (191)$$

Unfortunately, it is harder to derive a closed-form expression for c as function of σ for a general (non-infinite) value of K .

Figure 11 shows examples of kernels from the two families generated for this mapping between the parameters in the two families of temporal smoothing kernels for the limit case (181) when the number of temporal scale levels tends to infinity. As can be seen from the graphs, the kernels from the two families do to a first approximation share qualitatively largely similar properties. From a more detailed inspection, we can, however, note that the two families of kernels differ more in their temporal derivative responses in that (i) the temporal derivative responses are lower and temporally more spread out (less peaky) in the time-causal scale-space model based on first-order integrators coupled in cascade compared to Koenderink's scale-time model and that (ii) the temporal derivative responses are somewhat faster in the temporal scale-space model based on first-order integrators coupled in cascade.

A side effect of this analysis is that if we take the liberty of approximating the limit case of the time-causal kernels corresponding to a logarithmic distribution of the intermediate scale levels by the kernels in Koenderink's scale-time model with the parameters determined such that the first- and second-order temporal moments are equal, then we obtain the following approximate expression for the temporal location of the maximum point of the limit kernel

$$t_{max} \approx \frac{(c+1)^2 \sqrt{\tau}}{2\sqrt{2} \sqrt{(c-1)c^3}} = \delta \quad (192)$$

From the discussion above it follows that this estimate can be expected to be an overestimate of the temporal location of the maximum point of our time-causal kernels. This overestimate will, however, be better than the previously mentioned overestimate in terms of the temporal mean. For finite values of K not corresponding to the limit case, we can for higher accuracy alternatively estimate the position of the local maximum from δ in (186).

Figure 12 shows an additional quantification of the differences between these two classes of temporal smoothing kernels by showing how the skewness and the kurtosis measures vary as function of the distribution parameter c for the same mapping (181) between the parameters in the two families of temporal smoothing kernels. As can be seen from the graphs, both the skewness and the kurtosis measures are higher

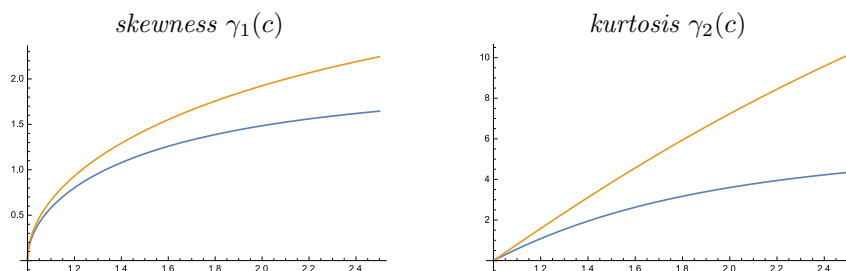


Figure 12: Comparison between the skewness and the kurtosis measures for the time-causal kernels corresponding to the limit case of K first-order integrators coupled in cascade when the number of temporal scale levels K tends to infinity (blue curves) and the corresponding temporal kernels in Koenderink's scale-time model (brown curves) with the parameter values determined such that the first- and second-order temporal moments are equal (equation (181)).

for the kernels in Koenderink's scale-time model compared to our time-causal kernels corresponding to first-order integrators coupled in cascade and do in these respect correspond to a larger deviation from a Gaussian behaviour over the temporal domain. (Recall that for a purely Gaussian temporal model all the cumulants of higher order than two are zero, including the skewness and the kurtosis measures.)

References

- [1] Adelson, E., Bergen, J.: Spatiotemporal energy models for the perception of motion. *J. Optical Society of America* **A 2**, 284–299 (1985)
- [2] Alvarez, L., Guichard, F., Lions, P.L., Morel, J.M.: Axioms and fundamental equations of image processing. *Arch. for Rational Mechanics* **123**(3), 199–257 (1993)
- [3] Babaud, J., Witkin, A.P., Baudin, M., Duda, R.O.: Uniqueness of the Gaussian kernel for scale-space filtering. *IEEE Trans. Pattern Analysis and Machine Intell.* **8**(1), 26–33 (1986)
- [4] Barbieri, D., Citti, G., Cocci, G., Sarti, A.: A cortical-inspired geometry for contour perception and motion integration. *Journal of Mathematical Imaging and Vision* **49**(3), 511–529 (2014)
- [5] van der Berg, E.S., Reyneke, P.V., de Ridder, C.: Rotational image correlation in the Gauss-Laguerre domain. In: *Third SPIE Conference on Sensors, MEMS and Electro-Optic Systems: Proc. of SPIE*, vol. 9257, pp. 92,570F–1–92,570F–17 (2014)
- [6] den Brinker, A.C., Roufs, J.A.J.: Evidence for a generalized Laguerre transform of temporal events by the visual system. *Biological Cybernetics* **67**(5), 395–402 (1992)
- [7] Cocci, C., Barbieri, D., Sarti, A.: Spatiotemporal receptive fields in V1 are optimally shaped for stimulus velocity estimation. *Journal of the Optical Society of America (JOSA A)* **29**(1), 130–138 (2012)
- [8] DeAngelis, G.C., Anzai, A.: A modern view of the classical receptive field: Linear and non-linear spatio-temporal processing by V1 neurons. In: L.M. Chalupa, J.S. Werner (eds.) *The Visual Neurosciences*, vol. 1, pp. 704–719. MIT Press (2004)
- [9] DeAngelis, G.C., Ohzawa, I., Freeman, R.D.: Receptive field dynamics in the central visual pathways. *Trends in Neuroscience* **18**(10), 451–457 (1995)
- [10] Duits, R., Burgeth, B.: Spatio-temporal scale-spaces. In: F. Gallari, A. Murli, N. Paragios (eds.) *Proc. Int. Conf. on Scale-Space Theories and Variational Methods in Computer Vision (SSVM 2007)*, *Lecture Notes in Computer Science*, vol. 4485, pp. 300–312. Springer (2007)
- [11] Duits, R., Felsberg, M., Florack, L., Platel, B.: α -scale-spaces on a bounded domain. In: L. Griffin, M. Lillholm (eds.) *Proc. Scale-Space Methods in Computer Vision (Scale-Space'03)*, *Lecture Notes in Computer Science*, vol. 2695, pp. 494–510. Springer, Isle of Skye, Scotland (2003)

- [12] Duits, R., Florack, L., de Graaf, J., ter Haar Romeny, B.: On the axioms of scale space theory. *J. of Mathematical Imaging and Vision* **22**, 267–298 (2004)
- [13] Fagerström, D.: Temporal scale-spaces. *Int. J. of Computer Vision* **2–3**, 97–106 (2005)
- [14] Fagerström, D.: Spatio-temporal scale-spaces. In: F. Gallari, A. Murli, N. Paragios (eds.) *Proc. Int. Conf. on Scale-Space Theories and Variational Methods in Computer Vision (SSVM 2007)*, *Lecture Notes in Computer Science*, vol. 4485, pp. 326–337. Springer (2007)
- [15] Faugeras, O., Toubol, J., Cessac, B.: A constructive mean-field analysis of multi-population neural networks with random synaptic weights and stochastic inputs. *Frontiers in Computational Neuroscience* **3**(1), 10.3389/neuro.10.001.2009 (2009)
- [16] Felsberg, M., Sommer, G.: The monogenic scale-space: A unifying approach to phase-based image processing in scale-space. *J. of Mathematical Imaging and Vision* **21**, 5–26 (2004)
- [17] Fleet, D.J., Langley, K.: Recursive filters for optical flow. *IEEE Trans. Pattern Analysis and Machine Intell.* **17**(1), 61–67 (1995)
- [18] Florack, L.M.J.: *Image Structure*. Series in Mathematical Imaging and Vision. Springer (1997)
- [19] Florack, L.M.J., ter Haar Romeny, B.M., Koenderink, J.J., Viergever, M.A.: Families of tuned scale-space kernels. In: G. Sandini (ed.) *Proc. European Conf. on Computer Vision (ECCV’92)*, *Lecture Notes in Computer Science*, vol. 588, pp. 19–23. Springer-Verlag, Santa Margherita Ligure, Italy (1992)
- [20] Florack, L.M.J., ter Haar Romeny, B.M., Koenderink, J.J., Viergever, M.A.: Scale and the differential structure of images. *Image and Vision Computing* **10**(6), 376–388 (1992)
- [21] Florack, L.M.J., ter Haar Romeny, B.M., Koenderink, J.J., Viergever, M.A.: Cartesian differential invariants in scale-space. *J. of Mathematical Imaging and Vision* **3**(4), 327–348 (1993)
- [22] Fourtes, M.G.F., Hodgkin, A.L.: Changes in the time scale and sensitivity in the ommatidia of limulus. *Journal of Physiology* **172**, 239–263 (1964)
- [23] Freeman, W.T., Adelson, E.H.: The design and use of steerable filters. *IEEE Trans. Pattern Analysis and Machine Intell.* **13**(9), 891–906 (1991)
- [24] Guichard, F.: A morphological, affine, and Galilean invariant scale-space for movies. *IEEE Trans. Image Processing* **7**(3), 444–456 (1998)
- [25] ter Haar Romeny, B. (ed.): *Geometry-Driven Diffusion in Computer Vision*. Series in Mathematical Imaging and Vision. Springer (1994)
- [26] ter Haar Romeny, B., Florack, L., Nielsen, M.: Scale-time kernels and models. In: *Proc. Int. Conf. Scale-Space and Morphology in Computer Vision (Scale-Space’01)*, *Lecture Notes in Computer Science*. Springer, Vancouver, Canada (2001)
- [27] Heeger, D.J.: Normalization of cell responses in cat striate cortex. *Visual Neuroscience* **9**, 181–197 (1992)
- [28] Hubel, D.H., Wiesel, T.N.: Receptive fields of single neurones in the cat’s striate cortex. *J Physiol* **147**, 226–238 (1959)
- [29] Hubel, D.H., Wiesel, T.N.: Receptive fields, binocular interaction and functional architecture in the cat’s visual cortex. *J Physiol* **160**, 106–154 (1962)
- [30] Hubel, D.H., Wiesel, T.N.: *Brain and Visual Perception: The Story of a 25-Year Collaboration*. Oxford University Press (2005)
- [31] Iijima, T.: Observation theory of two-dimensional visual patterns. Tech. rep., Papers of Technical Group on Automata and Automatic Control, IECE, Japan (1962)
- [32] Jhuang, H., Serre, T., Wolf, L., Poggio, T.: A biologically inspired system for action recognition. In: *International Conference on Computer Vision (ICCV’07)*, pp. 1–8 (2007)
- [33] Karlin, S.: *Total Positivity*. Stanford Univ. Press (1968)
- [34] Koch, C.: *Biophysics of Computation: Information Processing in Single Neurons*. Oxford University Press (1999)
- [35] Koenderink, J.J.: The structure of images. *Biological Cybernetics* **50**, 363–370 (1984)
- [36] Koenderink, J.J.: Scale-time. *Biological Cybernetics* **58**, 159–162 (1988)
- [37] Koenderink, J.J., van Doorn, A.J.: Receptive field families. *Biological Cybernetics* **63**, 291–298 (1990)

- [38] Koenderink, J.J., van Doorn, A.J.: Generic neighborhood operators. *IEEE Trans. Pattern Analysis and Machine Intell.* **14**(6), 597–605 (1992)
- [39] Laptev, I., Lindeberg, T.: Local descriptors for spatio-temporal recognition. In: Proc. ECCV'04 Workshop on Spatial Coherence for Visual Motion Analysis, *Lecture Notes in Computer Science*, vol. 3667, pp. 91–103. Springer, Prague, Czech Republic (2004)
- [40] Lindeberg, T.: Scale-space for discrete signals. *IEEE Trans. Pattern Analysis and Machine Intell.* **12**(3), 234–254 (1990)
- [41] Lindeberg, T.: Discrete derivative approximations with scale-space properties: A basis for low-level feature extraction. *J. of Mathematical Imaging and Vision* **3**(4), 349–376 (1993)
- [42] Lindeberg, T.: Effective scale: A natural unit for measuring scale-space lifetime. *IEEE Trans. Pattern Analysis and Machine Intell.* **15**(10), 1068–1074 (1993)
- [43] Lindeberg, T.: *Scale-Space Theory in Computer Vision*. Springer (1993)
- [44] Lindeberg, T.: Scale-space theory: A basic tool for analysing structures at different scales. *Journal of Applied Statistics* **21**(2), 225–270 (1994). Also available from <http://www.csc.kth.se/~tony/abstracts/Lin94-SI-abstract.html>
- [45] Lindeberg, T.: On the axiomatic foundations of linear scale-space. In: J. Sporring, M. Nielsen, L. Florack, P. Johansen (eds.) *Gaussian Scale-Space Theory: Proc. PhD School on Scale-Space Theory*, pp. 75–97. Springer, Copenhagen, Denmark (1996)
- [46] Lindeberg, T.: Linear spatio-temporal scale-space. In: B.M. ter Haar Romeny, L.M.J. Florack, J.J. Koenderink, M.A. Viergever (eds.) *Scale-Space Theory in Computer Vision: Proc. First Int. Conf. Scale-Space'97, Lecture Notes in Computer Science*, vol. 1252, pp. 113–127. Springer, Utrecht, The Netherlands (1997). Extended version available as technical report ISRN KTH NA/P-01/22-SE from KTH <http://www.nada.kth.se/cvap/abstracts/cvap257.html>
- [47] Lindeberg, T.: On automatic selection of temporal scales in time-casual scale-space. In: G. Sommer, J.J. Koenderink (eds.) *Proc. AFPAC'97: Algebraic Frames for the Perception-Action Cycle, Lecture Notes in Computer Science*, vol. 1315, pp. 94–113. Springer, Kiel, Germany (1997)
- [48] Lindeberg, T.: Edge detection and ridge detection with automatic scale selection. *Int. J. of Computer Vision* **30**(2), 117–154 (1998)
- [49] Lindeberg, T.: Feature detection with automatic scale selection. *Int. J. of Computer Vision* **30**(2), 77–116 (1998)
- [50] Lindeberg, T.: Scale-space. In: B. Wah (ed.) *Encyclopedia of Computer Science and Engineering*, pp. 2495–2504. John Wiley and Sons, Hoboken, New Jersey (2008)
- [51] Lindeberg, T.: Generalized Gaussian scale-space axiomatics comprising linear scale-space, affine scale-space and spatio-temporal scale-space. *J. of Mathematical Imaging and Vision* **40**(1), 36–81 (2011)
- [52] Lindeberg, T.: A computational theory of visual receptive fields. *Biological Cybernetics* **107**(6), 589–635 (2013)
- [53] Lindeberg, T.: Generalized axiomatic scale-space theory. In: P. Hawkes (ed.) *Advances in Imaging and Electron Physics*, vol. 178, pp. 1–96. Elsevier (2013)
- [54] Lindeberg, T.: Scale selection properties of generalized scale-space interest point detectors. *J. of Mathematical Imaging and Vision* **46**(2), 177–210 (2013)
- [55] Lindeberg, T.: Image matching using generalized scale-space interest points. *Journal of Mathematical Imaging and Vision* (2014). Doi:10.1007/s10851-014-0541-0
- [56] Lindeberg, T.: Separable time-causal and time-recursive receptive fields. In: Proc. Scale-Space and Variational Methods for Computer Vision (SSVM 2015), *Springer LNCS*, vol. 9087 (2015). In press, DOI:10.1007/978-3-319-18461-6_8, preprint at arXiv:1504.01502
- [57] Lindeberg, T., Bretzner, L.: Real-time scale selection in hybrid multi-scale representations. In: L. Griffin, M. Lillholm (eds.) *Proc. Scale-Space Methods in Computer Vision (Scale-Space'03), Lecture Notes in Computer Science*, vol. 2695, pp. 148–163. Springer, Isle of Skye, Scotland (2003)
- [58] Lindeberg, T., Fagerström, D.: Scale-space with causal time direction. In: Proc. European Conf. on Computer Vision (ECCV'96), vol. 1064, pp. 229–240. Springer, Cambridge, UK (1996)
- [59] Lindeberg, T., Friberg, A.: Idealized computational models of auditory receptive fields. *PLOS ONE* (2015). In press, doi:10.1371/journal.pone.0119032, preprint at arXiv:1404.2037

- [60] Mattia, M., Guidice, P.D.: Population dynamics of interacting spiking neurons. *Physics Review E* **66**(5), 051,917 (2002)
- [61] Miao, X., Rao, R.P.N.: Learning the Lie group of visual invariance. *Neural Computation* **19**, 2665–2693 (2007)
- [62] Omurtag, A., Knight, B.W., Sirovich, L.: On the simulation of large populations of neurons. *Journal of Computational Neuroscience* **8**, 51–63 (2000)
- [63] Pauwels, E.J., Fiddelaers, P., Moons, T., van Gool, L.J.: An extended class of scale-invariant and recursive scale-space filters. *IEEE Trans. Pattern Analysis and Machine Intell.* **17**(7), 691–701 (1995)
- [64] Perona, P.: Steerable-scalable kernels for edge detection and junction analysis. *Image and Vision Computing* **10**, 663–672 (1992)
- [65] Rivero-Moreno, C.J., Bres, S.: Spatio-temporal primitive extraction using Hermite and Laguerre filters for early vision video indexing. In: *Image Analysis and Recognition, Springer LNCS*, vol. 3211, pp. 825–832 (2004)
- [66] Schoenberg, I.J.: Über Variationsvermindernde Lineare Transformationen. *Mathematische Zeitschrift* **32**, 321–328 (1930)
- [67] Schoenberg, I.J.: Contributions to the problem of approximation of equidistant data by analytic functions. *Quarterly of Applied Mathematics* **4**, 45–99 (1946)
- [68] Schoenberg, I.J.: On totally positive functions, Laplace integrals and entire functions of the Laguerre-Pòlya-Schur type. *Proc. National Academy of Sciences* **33**, 11–17 (1947)
- [69] Schoenberg, I.J.: Some analytical aspects of the problem of smoothing. In: *Courant Anniversary Volume, Studies and Essays*, pp. 351–370. New York (1948)
- [70] Schoenberg, I.J.: On Pòlya frequency functions. ii. Variation-diminishing integral operators of the convolution type. *Acta Sci. Math. (Szeged)* **12**, 97–106 (1950)
- [71] Schoenberg, I.J.: On smoothing operations and their generating functions. *Bull. Amer. Math. Soc.* **59**, 199–230 (1953)
- [72] Shabani, A.H., Clausi, D.A., Zelek, J.S.: Improved spatio-temporal salient feature detection for action recognition. In: *British Machine Vision Conference (BMVC'11)*, pp. 1–12. Dundee, U.K. (2011)
- [73] Simoncelli, E.P., Freeman, W.T., Adelson, E.H., Heeger, D.J.: Shiftable multi-scale transforms. *IEEE Trans. Information Theory* **38**(2) (1992)
- [74] Tschirsich, M., Kuijper, A.: Notes on discrete Gaussian scale space. *J. of Mathematical Imaging and Vision* **51**, 106–123 (2015)
- [75] U. Sharma, U., Duits, R.: Left-invariant evolutions of wavelet transforms on the similitude group. *Applied and Computational Harmonic Analysis* (2014)
- [76] Valois, R.L.D., Cottaris, N.P., Mahon, L.E., Elfer, S.D., Wilson, J.A.: Spatial and temporal receptive fields of geniculate and cortical cells and directional selectivity. *Vision Research* **40**(2), 3685–3702 (2000)
- [77] Weickert, J.: *Anisotropic Diffusion in Image Processing*. Teubner-Verlag, Stuttgart, Germany (1998)
- [78] Weickert, J., Ishikawa, S., Imiya, A.: On the history of Gaussian scale-space axiomatics. In: J. Sparring, M. Nielsen, L. Florack, P. Johansen (eds.) *Gaussian Scale-Space Theory: Proc. PhD School on Scale-Space Theory*, pp. 45–59. Springer, Copenhagen, Denmark (1997)
- [79] Weickert, J., Ishikawa, S., Imiya, A.: Linear scale-space has first been proposed in Japan. *J. of Mathematical Imaging and Vision* **10**(3), 237–252 (1999)
- [80] Willems, G., Tuytelaars, T., van Gool, L.: An efficient dense and scale-invariant spatio-temporal interest point detector. In: *Proc. ECCV'08, Lecture Notes in Computer Science*, vol. 5303, pp. 650–663. Springer, Marseille, France (2008)
- [81] Witkin, A.P.: Scale-space filtering. In: *Proc. 8th Int. Joint Conf. Art. Intell.*, pp. 1019–1022. Karlsruhe, Germany (1983)
- [82] Yuille, A.L., Poggio, T.A.: Scaling theorems for zero-crossings. *IEEE Trans. Pattern Analysis and Machine Intell.* **8**, 15–25 (1986)
- [83] Zelnik-Manor, L., Irani, M.: Event-based analysis of video. In: *Proc. Computer Vision and Pattern Recognition*, pp. II:123–130. Kauai Marriott, Hawaii (2001)